

Detection and Evaluation of Clusters within Sequential Data

Alexander Van Werde, Albert Senen–Cerde, Gianluca Kosmella, Jaron Sanders



Abstract—Motivated by theoretical advancements in dimensionality reduction techniques we use a recent model, called Block Markov Chains, to conduct a practical study of clustering in real-world sequential data. Clustering algorithms for Block Markov Chains possess theoretical optimality guarantees and can be deployed in sparse data regimes. Despite these favorable theoretical properties, a thorough evaluation of these algorithms in realistic settings has been lacking.

We address this issue and investigate the suitability of these clustering algorithms in exploratory data analysis of real-world sequential data. In particular, our sequential data is derived from human DNA, written text, animal movement data and financial markets. In order to evaluate the determined clusters, and the associated Block Markov Chain model, we further develop a set of evaluation tools. These tools include benchmarking, spectral noise analysis and statistical model selection tools. An efficient implementation of the clustering algorithm and the new evaluation tools is made available together with this paper.

Practical challenges associated to real-world data are encountered and discussed. It is ultimately found that the Block Markov Chain model assumption, together with the tools developed here, can indeed produce meaningful insights in exploratory data analyses despite the complexity and sparsity of real-world data.

1 Introduction

Modern data often consists of observations that were obtained from some complex process, and that became available sequentially. The specific order in which the observations occur often matters: future observations correlate typically with past observations. By identifying a relation between subsequent observations within sequential data one may hope to gain insight into the underlying complex process. The high-dimensional nature of modern data however can make understanding the sequential structure difficult. Many algorithms which one may want to apply to the data namely slow down to an infeasible degree in a high-dimensional regime. Further, human interpretation of the data may become tedious. To avoid these issues it is desirable to identify a latent structure which respects the sequential structure but has reduced dimensions.

In this paper we are concerned with uncovering lower-dimensional structures within sequential data when this latent structure is hidden from the observer but still detectable from the specific sequence of observations. Practical tools

for the discovery, evaluation, and presentation of the lower-dimensional structures from real-world sequential data are developed and applied. The term “real-world data” is here in contrast to synthetic data. For synthetic data one namely often has prior knowledge concerning a ground-truth latent structure, and this facilitates evaluation of latent structures which are output by an algorithm. Such prior knowledge is not available for real-world data, complicating the evaluation.

We focus on a popular class of methods for discovering latent structure in datasets: *clustering algorithms*. Clustering algorithms work by clustering together data points from a dataset that are “similar” in some sense. If for instance data has a geometric structure for which a notion of distance is applicable then one may call two points similar if their distance is small. This distance-based notion of similarity can be leveraged with the well-known K -means algorithm for clustering point clouds. If instead the data has a graph structure then it is natural to call two vertices of the graph similar if they connect to other vertices in similar ways. This connection-based notion is made rigorous in the Stochastic Block Model for random graphs.

A natural notion of similarity for sequential observations, whose order matters, may similarly be given by the following informal criterion: “two observations are similar if and only if they transition into other observations in similar ways.” This transition-based notion is made formal in Block Markov Chains (BMCs). Specifically, the BMC-model assumes that the observations are the states of a Markov Chain (MC) in which the state space can be partitioned in such a manner that the transition rate between two states only depends on the parts of the partition (clusters) in which these two states lie.

The problem of clustering the observations in a single sequence of observations of a BMC was recently investigated theoretically [1], [2]. For example, given a sample path generated by a BMC, the authors of [2] provide information-theoretic thresholds below which exact clustering is impossible because insufficient data is available. The authors also provide a clustering algorithm which can provably recover the underlying clusters whenever these conditions are satisfied. The clustering algorithm consists of two steps. First, an initial guess for the underlying cluster structure is found by means of a *spectral initialization*. Here the term spectral refers to the fact that singular vectors of a random matrix associated to the sample path are employed. These singular vectors are used to construct a low-rank approximation of the random matrix after which a K -means algorithm is applied. Second, the initial guess for

The authors are with the Faculty of Mathematics and Computer Science, Eindhoven University of Technology, Groene Loper 5, 5612 AZ Eindhoven, The Netherlands.

E-mail: a.van.werde@tue.nl, a.senen.cerde@tue.nl, g.k.kosmella@tue.nl, jaron.sanders@tue.nl

the cluster structure is refined by means of an *improvement algorithm* that reconsiders the sequence of observations and performs a greedy, local maximization of the log-likelihood function of the BMC model.

A broad study on the performance of this clustering algorithm for sequential data obtained from real-world processes was however not provided. We tackle this problem by investigating the clustering algorithm under a variety of scenarios, and thus demonstrating its applicability in real-world data. This is the main contribution of the present paper. Evaluating the actual performance of such clustering algorithm in a real-world scenario is however a nontrivial task since the latent cluster structure is unknown, as opposed to a scenario where data is generated synthetically. Hence, we also propose a set of tools used for evaluation of the quality of the clusters and the BMC model. We go, therefore, a step beyond clustering benchmark evaluation and use statistical tools to assess the validity of the BMC assumption in the data.

Our goal is here not to compare the performance of the BMC clustering algorithm relative to other algorithms. A comparison would namely only be fair if both algorithms have access to the same amount of training data. Now remark that the BMC algorithm is explicitly designed to manage in sparse regimes where the amount of data is small. On the other hand most model-free algorithms, such as those based on deep learning, perform optimally in a regime where one has access to large amounts of training data. A comparison would consequently be vacuous; its outcome mainly being determined by the choice of the amount of training data. Our goal is rather to supplement the theoretical understanding of the BMC-based algorithm with a practical viewpoint.

In order to practically evaluate the clustering algorithm for BMCs, we investigate the following questions:

- How can the BMC model practically aid in data exploration of nonsynthetic sequential data obtained from real-world data?
- Can the quality of the found clusters be evaluated when no ground-truth clustering is known?
- How can one statistically decide whether the BMC model is an appropriate model for the sequence of observations? How can it be detected that either a simpler model than a BMC would suffice, or a richer model is required?
- Can the algorithm be expected to give meaningful results despite the sparsity and complexity of real-world data? Are the clustering algorithms robust to model violations?

To obtain insight into these questions, we develop practical tools for evaluating the merit of a detected clustering, which we then apply to several data sets. These evaluation tools are designed to cope with the aforementioned fact that ground-truth clusters are not known to us. The datasets which we consider are diverse as they come from the fields of microbiology, natural language processing, ethology, and finance. Specifically, we investigate sequences of:

- a. Codons in human Deoxyribonucleic Acid (DNA).
- b. Words in Wikipedia articles.
- c. Global Positioning System (GPS) data describing the movement of bison in a field.
- d. Companies in the Standard and Poor's 500 (S&P500) with the highest daily return.

On each dataset we apply the BMC clustering algorithm to uncover underlying clusters, and we evaluate these clusters using the collection of tools which are developed in the present paper. It is here found that the BMC model indeed aids in exploratory data analyses of real-world sequential data.

For example, in DNA the algorithm leads us to rediscover phenomena which are known in the biological community as codon-pair bias and dinucleotide bias. In the text-based sequential data we find that the BMC-based improvement algorithm improves performance on downstream natural language processing tasks. The model evaluation tools of the present paper are here found to be informative. They namely uncover some model violations which are suggestive for future methodological expansion. Our findings in the GPS data are particularly striking. There, a scatter plot of the data gives rise to a picture which is difficult to interpret. After clustering, a picture can be displayed which provides significantly more insight; compare Figure 3 and Figure 6. It is further notable that the sequential structure of the data gives rise to geographical features which would have been difficult, if not impossible, to extract based on solely a distance-based notion of similarity as is employed in K -means. The S&P500 dataset gives the least clear conclusions out of the four datasets but is a good illustrative example for our evaluation tools in a difficult setting. The difficulty of this dataset is due to the combination of sparsity and a nuisance factor. With these different examples, along with the evaluation tools developed, we answer positively the highlighted questions posed previously, and we conclude that the BMC-based clustering can be successfully applied to real-world sequential data.

Let us finally contemplate the practical implication of our findings as it pertains to using clustering within sequential data as a method to speed up a subsequent optimization procedure. Consider that canonical machine learning algorithms that one would like to apply to sequential data, such as Q -learning or *SARSA*-learning, slow down to an impractical degree if the observations are from a high-dimensional state space. By solving such learning problems on an accurate lower-dimensional representation of the state space, the numerical complexity can be reduced dramatically [3], [4]. The present paper suggest that future integration of clustering in sequential data applications such as natural language processing and machine learning is indeed practically feasible.

Structure of this paper

We introduce the problem of clustering in sequential data in Section 2. We describe the BMC as well as other models that appear in our experiments in Section 3, and briefly discuss the advantages of a model-based approach. Next, we give an overview of related literature in Section 4, and we introduce the clustering algorithm in Section 5. We describe there also our C++ implementation of this clustering algorithm, which we made publicly available as a Python library. Section 6 describes practical tools to evaluate clusters found in datasets in the absence of knowledge on the underlying ground truth. Section 7 introduces the datasets and explains our preprocessing procedures; Sections 8, 9 then extensively evaluate the clusters. Finally, Section 10 concludes with a brief summary.

2 Problem formulation

We suppose that we have obtained an ordered sequence of $\ell \in \mathbb{N}_+$ discrete observations

$$X_{1:\ell} := X_1 \rightarrow X_2 \rightarrow \dots \rightarrow X_\ell \quad (1)$$

from some complex process. The observations can be real numbers (one- or higher-dimensional) or abstract system states; as long as the observations come from a finite set. We assume specifically that there exists a number $n \in \mathbb{N}_+$ such that the sequence satisfies $X_t \in [n] := \{1, \dots, n\}$ for $t \in [\ell]$. Here, n can be interpreted as the number of distinct, discrete observations that are possible.

Given such ordered sequence of observations, we wonder whether there exists a map $\sigma_n : [n] \rightarrow [K]$ with $1 \leq K \leq n$ an integer, such that the ordered sequence

$$\sigma_n(X_{1:\ell}) := \sigma_n(X_1) \rightarrow \sigma_n(X_2) \rightarrow \dots \rightarrow \sigma_n(X_\ell) \quad (2)$$

captures dynamics of the underlying complex process. Observe that the map σ_n defines K clusters:

$$\mathcal{V}_k := \{i \in [n] \mid \sigma_n(i) = k\} \quad (3)$$

for $k \in [K]$. Furthermore, $\mathcal{V}_k \cap \mathcal{V}_l = \emptyset$ whenever $k \neq l$ and $\cup_{k=1}^K \mathcal{V}_k = [n]$.

The clusters $\mathcal{V}_1, \dots, \mathcal{V}_K$ are particularly interesting when $K \ll n$. In such a case the *clustered* process $\{\sigma_n(X_t)\}_t$ lives in a much smaller observation space than the original process $\{X_t\}_t$. The reduction may then prove to be beneficial for computational tasks since the time complexity of some algorithms depends on the size of the observation space. If (2) furthermore indeed captures the dynamics of the complex process, then it is not unreasonable to expect that the clusters \mathcal{V}_k could themselves be meaningful thus allowing for human interpretation of the data.

3 Models

3.1 Main model: BMC

The main model in this paper is given by BMCs. Formally, a *1st-order BMC* is a discrete-time stochastic process $\{X_t\}_{t \geq 0}$ on a state space $\mathcal{V} := [n]$ that satisfies not only the MC property

$$\begin{aligned} \mathbb{P}[X_{t+1} = j \mid X_t = i, X_{t-1} = i_{t-1}, \dots, X_0 = i_0] \\ = \mathbb{P}[X_{t+1} = j \mid X_t = i] \forall j, i, i_{t-1}, \dots, i_0 \in [n]; \end{aligned} \quad (4)$$

but also that there exists a cluster assignment map $\sigma_n : [n] \rightarrow [K]$ such that there exists a stochastic matrix $p \in \mathbb{R}^{K \times K}$ with

$$P_{i,j} := \mathbb{P}[X_{t+1} = j \mid X_t = i] = \frac{p_{\sigma_n(i), \sigma_n(j)}}{\#\mathcal{V}_{\sigma_n(j)}}. \quad (5)$$

Here \mathcal{V}_k is defined as in (3). The $p_{k,l} \in [0, 1]$ are called the *cluster transition probabilities* and satisfy $\sum_{l=1}^K p_{k,l} = 1$ for $k \in [K]$. The matrix $(P_{i,j})_{i=1, j=1}^n$ is called the *state transition matrix*. Figure 1 depicts a BMC on $K = 3$ clusters.

The BMC-model can be viewed as an ideal case for the setup of (2). The reduced process $\{\sigma_n(X_t)\}_t$ namely not only captures *some* part of the dynamics of the true process but rather *all* of the order-dependent dynamics. Indeed, observe that for any $t > 1$ it holds that conditional on $\sigma_n(X_t) = k$ the observation X_t is chosen uniformly at random in the cluster \mathcal{V}_k . The previous state X_{t-1} hence influences the next cluster

$\sigma_n(X_t)$ but does not provide any further information about the precise element in $\mathcal{V}_{\sigma_n(X_t)}$.

If the MC associated to p is ergodic, then the BMC has a unique *state equilibrium distribution* $\Pi \in [0, 1]^n$. This state equilibrium distribution moreover has the symmetry property that Π_j only depends on the cluster assignment $\sigma_n(j)$ for any $j \in [n]$. That is, for any initial value $i_0 \in [n]$

$$\begin{aligned} \Pi_j &:= \lim_{t \rightarrow \infty} \mathbb{P}[X_t = j \mid X_0 = i_0] \\ &= \frac{1}{\#\mathcal{V}_{\sigma_n(j)}} \lim_{t \rightarrow \infty} \mathbb{P}[\sigma_n(X_t) = \sigma_n(j) \mid \sigma_n(X_0) = \sigma_n(i_0)] \\ &=: \frac{\pi_{\sigma_n(j)}}{\#\mathcal{V}_{\sigma_n(j)}}. \end{aligned} \quad (6)$$

Note that $\pi \in [0, 1]^K$ is here the cluster equilibrium distribution of the MC on $[K]$ which is associated to the cluster transition matrix p . One can characterize π as the unique column vector satisfying $\pi^T p = \pi$ and $\sum_{k=1}^K \pi_k = 1$.

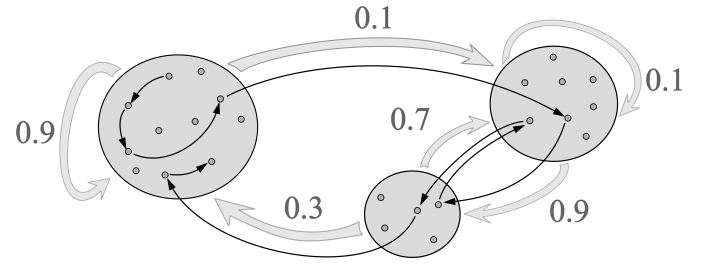


Fig. 1. A visualization of a BMC with $K = 3$ clusters and $p = [[0.9, 0.1, 0], [0, 0.1, 0.9], [0.3, 0.7, 0]]$. The thick arrows visualize to the cluster transition probabilities $p_{k,l}$, while the thin arrows visualize the transitions of a sample path $\{X_t\}_t$. Figure courtesy of [5].

3.2 Other models for experimentation

Recall that one of our goals is to develop tools which aid in evaluating whether the BMC model is an appropriate model. In this setting it is oftentimes useful to have some alternative models to compare with. The models that we have used are collected here for easy reference.

3.2.1 0th-order BMCs

Let $K \in [n]$ and consider an arbitrary probability distribution $\eta : [K] \rightarrow [0, 1]$. A *0th-order BMC* is then a BMC with cluster transition matrix $p_{k,l} := \eta_l$ for all $k, l \in [K]$. The 0th-order BMC will serve as a benchmark to assert whether the structures we find are actually due to the sequential nature of the process and do not admit a simpler explanation.

Namely, observe that in a 0th-order BMC each next sample X_{t+1} is independent of the previous sample X_t . A 0th-order BMC therefore generates sequences of independent and identically distributed random variables. This is contrary to a 1st-order BMC, which generates a sequence of dependent random variables. The probability of a specific observation does depend on the cluster of the observation, and specifically is identical for every observation within that cluster.

3.2.2 rth-order MCs

Conversely, one can also consider models with higher-order dependencies than the 1st-order BMC has.

Consider a discrete-time stochastic process $\{Y_t\}_{t=1}^\ell$ (not necessarily a MC) that satisfies $Y_t \in [n]$ for some $n \in \mathbb{N}_+$.

We say that $\{Y_t\}_{t \geq 1}$ is an r th-order MC if and only if for all $t \in [\ell - r]$, all $i^r = (i_1, \dots, i_r) \in [n]^r$ and $j \in [n]$,

$$\mathbb{P}[Y_{t+1} = j \mid Y_t = i_r, Y_{t-1} = i_{r-1}, \dots, Y_{t-r+1} = i_1, \\ Y_{t-r} = s_{t-r}, \dots, Y_1 = s_1] \quad (7)$$

$= \mathbb{P}[Y_{t+1} = j \mid Y_t = i_r, Y_{t-1} = i_{r-1}, \dots, Y_{t-r+1} = i_1] =: P_{i^r, j}^r$
for some transition matrix $P^r \in [0, 1]^{n^r \times n}$.

3.2.3 Perturbed BMCs

Finally, we consider an alternative model which concerns the scenario where a BMC captures the dynamics only partially. Specifically, a *perturbed BMC* mixes a 1st-order BMC on $[n]$ that has transition matrix P_{BMC} with a generic 1st-order MC on $[n]$ that has transition matrix Δ by consideration of the MC with transition matrix

$$P_{\text{Perturbed}} := (1 - \varepsilon)P_{\text{BMC}} + \varepsilon\Delta. \quad (8)$$

The parameter $\varepsilon \in [0, 1]$ measures how many transitions are affected by the non-BMC part Δ .

Concretely: let $\{B_t\}_{t \geq 0}$ denote a sequence of independent, identically distributed Bernoulli random variables, each taking the value 1 with probability ε . The perturbed BMC corresponds to the MC $\{X_t^\varepsilon\}_{t \geq 0}$ whose conditional transition probabilities are given by

$$\mathbb{P}[X_{t+1}^\varepsilon = j \mid X_t^\varepsilon = i, B_t = b] = \begin{cases} P_{\text{BMC}, ij} & \text{if } b = 0, \\ \Delta_{ij} & \text{otherwise.} \end{cases} \quad (9)$$

In other words, a sequence $X_0^\varepsilon \rightarrow \dots \rightarrow X_\ell^\varepsilon$ from the perturbed BMC is generated by randomly selecting either the transition matrix P_{BMC} of a 1st-order BMC, or the transition matrix Δ of some other 1st-order MC, for each transition. Whenever we use a perturbed BMC, we specify Δ on the spot.

3.3 Concerning model misspecification

It is unlikely that the complex process $\{X_t\}_t$ in (1) is exactly a BMC. One may consequently wonder about the dangers of model misspecification:

- Is the clustering algorithm robust to violations of the model assumption?
- When concerned with executing a downstream task on $X_{1:\ell}$, does the BMC model assumption provide any benefit when compared to models with fewer assumptions?

In this regard we would like to point out that the data which we consider is not only complex but oftentimes also sparse. Let us illustrate the principle by a numerical experiment whose precise setup may be found in Supplement 12.

To model a violation of the model assumptions while retaining a sensible notion of ground-truth communities we considered the perturbed BMC model as defined in Section 3.2.

Concerning (a), we find that for small perturbation levels ε it is still possible to exactly recover the underlying clusters based on the construction of the algorithm; see Figure 2(a).

Concerning (b), we consider the scenario where the goal is to estimate the underlying transition kernel P of a Markovian process based on a sample path of length ℓ ; see Figure 2(b). We find that clustering worsens performance when ℓ is large because a lack of expressivity: the true kernel P is not exactly a BMC-kernel. On the other hand, when ℓ is small, the clustering improves performance. This is because the reduction

in the number of parameters makes the algorithm less prone to overfitting. The answer to (b) is thus that it can be advantageous to rely on the BMC model assumption when data is sparse.

4 Related literature

This section provides references that theoretically study the problem of clustering in BMCs and MCs, which have taken inspiration from references on the problem of community detection in random graphs. We also provide related references on clustering and time-series, as well as on state space reduction in decision theoretical problems. Finally, we give references on statistical tools that we employ.

Clustering in BMCs and MCs

Cluster detection in BMCs was studied theoretically in [1], [2]. This research has yielded an algorithm that provably detects clusters from the shortest sample paths whenever possible [2]. As evident from the proofs, studying the spectrum of BMC can yield sharp bounds for recoverability [2]. Spectral properties of the random matrices constructed from sample paths of BMCs were investigated further in [6], [5]. The more recent paper [5] proves convergence of a bulk of singular values to a limiting distribution in the dense regime $\ell = \Theta(n^2)$; a result that we use and refine in our experiments (see Section 6.4).

Other related clustering algorithms that also use spectral decompositions to learn low-rank structures from trajectories of MCs are studied in [7], [8]. Finally, for scenarios in which observations of a dynamical system are switched by a MC with low-rank structure, [9] provides a method for the problem of recovering a latent transition model. A similar objective is considered in [10] for long sample paths.

Community detection in random graphs

Community detection in random graphs, such as those produced by the Stochastic Block Model, is an active area of research. The distinction with clustering in BMCs is that the vertices within a single observation of a random graph are clustered, instead of the observations within sequential data. We refer the reader to [11] for an extensive overview on cluster recovery within the context of the Stochastic Block Model, and to [12] for an overview on community detection in graphs.

Other clustering of sequential data

In the reviews [13], [14], research that relates to both clustering and time-series/sequential data is divided into three categories. Clustering between different time-series is called “whole-time-series clustering.” Survey papers include [14], [15]. Another category is clustering of subsequences of a time-series, where individual time-series are extracted via a sliding window. In 2003 [16] it was shown that the algorithms present at that time extracted essentially random and therefore meaningless clusters, because they relied on assumptions unlikely to be met by non-synthetic data. The papers [17], [18] are contributions to seeking to obtain meaningful subsequence time-series clustering. Finally, there is clustering states of within a time-series, which is called “time-point clustering,” under which for example problems like segmenting an n -element sequence into k segments, which can come from h different sources, fall; see e.g. [19]. Other examples referenced in this category are [20], [21]. This category is closest to the clustering algorithm that we employ.

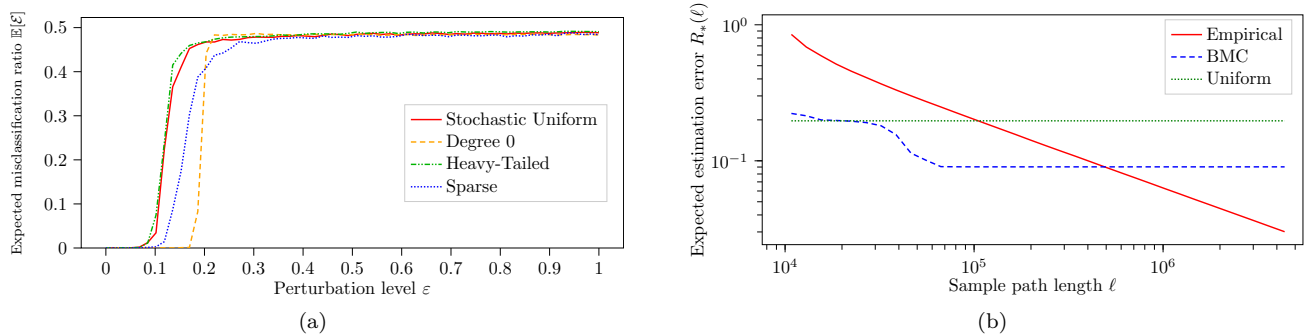


Fig. 2. (a) The expected proportion of states which are misclassified in terms of the perturbation level ε for four different perturbation models Δ and a sample path of length $\ell_n = \lfloor 30n \ln(n) \rfloor$ with a state space of and of size $n = 500$. (b) Estimated expected estimation error $R_*(\ell) := \mathbb{E}[\|P - \hat{P}_*(\ell)\|]$ for three different estimators. The ground-truth model in this experiment was a perturbed BMC with a heavy-tailed perturbation of strength $\varepsilon = 0.05$ on a state space of size $n = 1000$. In red: the empirical estimator $\hat{P}_{\text{Empirical}}$ which is the maximum likelihood estimator for a Markov chain with no additional assumptions. In blue: the BMC estimator \hat{P}_{BMC} . In green: the trivial estimator $\hat{P}_{\text{Uniform},ij} := 1/n$ which does not even use the data. Let us emphasize that the precise values in (a) and (b) depend on the precise parameters of the BMC which was perturbed. The general shape of the curves is expected to generalize but the precise numbers, e.g. that a perturbation up to $\varepsilon \approx 0.1$ is tolerable, will depend on the specifics.

State space reduction in decision theoretical problems

Studying clustering in MCs is motivated by the necessity for effective state space reduction techniques in decision theoretical problems, for example in Reinforcement Learning, Markov Decision Processes, and Multi-Armed Bandit problems. It is for example known that learning a latent space reduces regret in Multi-Armed Bandit problems [22], [23]. State aggregation and low rank approximations methods have been studied for Markov Decision Processes as well as Reinforcement Learning, see [24] and [25], [26], [27], respectively. The idea to cluster states in Reinforcement Learning based on the process' trajectory was first explored in the seminal papers [3], [4].

A few related experiments from the fields of microbiology, natural language processing, ethology, and finance

The first application of a MC model was by Andrei Markov, as he investigated a sequence of 20000 letters in A. S. Pushkin's poem "Eugeny Onegin" [28]. Since, MCs and hidden Markov models have been used in natural language processing [29].

Clustering in DNA, specifically clustering the sequence of nucleotides or the sequence of codons as a MC has been demonstrated [30], [31], [32], the current paper is the first time that a BMC was used for this task.

Using similar means as in the animal movement data in this paper, GPS coordinate sequences for New York City taxi trips are investigated in [1], [8], [5]. For both examples the low-dimensional representation reveals insight into taxi customer and animal movement behavior, respectively. The taxi trip data is however of quite different nature compared to the animal movement data, because in the taxi trip data far away entrance and drop-off locations can constitute a transition, while in the animal movement the transitions between states are only due to an animal moving from one area to another in a time intervals of roughly not more than an hour.

In [33] the transition between the Dow Jones closing prices are described as a MC close to equilibrium. Further references for MC models in finance include [34], [35]. Other Markovian models, like Hidden Markov Models, are also often used in the analysis of financial data; see for example [36].

Related statistical tools

Based on a likelihood ratio test statistic and a chi-square test statistic, [37] tests if two MCs on the same state space have the same transition matrix. The same problem is considered in [38] by considering a divergence test statistic. Further results are discussed in [39, §3.4.2].

Testing for the order of a MC can be done by the chi-square- and likelihood ratio-test statistic [37] and using ϕ -divergence test statistics [40]. Further hypothesis tests for Markovian models with random time observations are considered in [41] and specifically a goodness-of-fit test on the distribution is described. For selection of the order of a MC, general information criteria may also be used [42], [43], [44].

5 Clustering algorithm

In this section we describe the clustering algorithm from [2] which was designed to infer the map σ_n from the sample path of a BMC. The reason we use this particular clustering algorithm is that it has a mathematical guarantee that it can recover the clusters of BMCs accurately *even if* the number of observations ℓ is small compared to the number of possible transitions n^2 . This is useful for our purposes because observations are generally noisy and few in practice.

The clustering algorithm in [2] first constructs an *empirical frequency matrix* \hat{N} element-wise from the sequence of observations $X_{1:\ell}$: for $i, j \in [n]$,

$$\hat{N}_{ij} := \sum_{t=1}^{\ell-1} \mathbb{1}[X_t = i, X_{t+1} = j]. \quad (10)$$

Depending on the *sparsity* of the frequency matrix characterized by the ratio ℓ/n^2 , regularization is applied by *trimming*: all entries of rows and columns of \hat{N} corresponding to a desired number of states with the largest degrees, which we denote by Γ , are set to zero. The clustering algorithm then executes two steps on the resulting *trimmed frequency matrix* \hat{N}_Γ :

Step 1. Initialize with a spectral clustering algorithm.

Step 2. Iterate with a cluster improvement algorithm.

We provide pseudocode for these algorithms in Supplement 11.

Given some initial guess, here provided by a spectral algorithm, the cluster improvement algorithm consists of local

optimization of a log-likelihood function by a hill climbing procedure. The state space $[n]$ and the number of clusters K are kept fixed which means that the free parameters are the cluster transition matrix $p \in \{q \in [0, 1]^{K \times K} : \forall k, \sum_l q_{k,l} = 1\}$ and the cluster assignment map $\sigma_n : [n] \rightarrow [K]$. Given an observation sequence $X_{1:\ell}$, the log-likelihood of the BMC-model is given by

$$\hat{\mathcal{L}}(X_{1:\ell} | p, \sigma_n) := \sum_{t=1}^{\ell-1} \ln \frac{p_{X_t, X_{t+1}}}{\#\mathcal{V}_{\sigma_n}(X_{t+1})}. \quad (11)$$

The reason that this two-step procedure is used instead of directly maximizing (11), is that finding the global maximizer of (11) is numerically infeasible. Indicative of this numerical complexity is the fact that the number of possible partitions σ_n , given by the *partition function* $\zeta(n)$, grows exponentially as n increases

$$\zeta(n) \sim (4n\sqrt{3})^{-1} \exp(\pi\sqrt{2n/3}). \quad (12)$$

The fact that the hill climbing procedure, which is computationally tractable, succeeds at exactly (resp. accurately) recovering the true underlying parameters when initialized with a spectral clustering is formally established in [2] in the asymptotic regime where $\ell = \omega(n \log n)$ (resp. $\ell = \omega(n)$).

5.1 BMCToolkit: A C++ library and Python module

We have programmed a Dynamic-link library (DLL) in C++, called *BMCToolkit*, that can simulate and analyse trajectories of BMCs. Among other functionalities, the DLL is able to calculate both cluster and state variants of the equilibrium distribution, frequency matrix, and transition matrix of a BMC; to compute the difference between two clusters and the spectral norm; to estimate the parameters of a BMC from a sample path; to execute the spectral clustering algorithm and the cluster improvement algorithm; to generate sample paths and trimmed frequency matrices; and to relabel clusters according to the size or the equilibrium probability of a cluster.

The DLL utilizes *Eigen*, a high-level DLL for linear algebra, matrix, and vector operations; and the *Sparse Eigenvalue Computation Toolkit as a Redesigned ARPACK*, a DLL for large-scale eigenvalue problems built on top of *Eigen*. The mathematical components of *BMCToolkit* were validated through functional testing using Microsoft’s Native Unit Test Framework. The performance of the numerical components of *BMCToolkit* were finally benchmarked using *Benchmark*, Google’s microbenchmark support library. Our source code can be found at <https://gitlab.tue.nl/acss/public/detection-and-evaluation-of-clusters-within-sequential-data>.

We also created a Python module called *BMCToolkit*, and made it available at <https://pypi.org/project/BMCToolkit/>. This Python module distributes the DLL mentioned above and includes an easy-to-use Python interface. When compiling *BMCToolkit*, we made sure to instruct the Microsoft Visual C++ compiler to activate the *OpenMP* extension to parallelize the simulation across Central Processing Units and so that *Eigen* could parallelize matrix multiplications (`/openmp`); to apply maximum optimization (`/O2`); to enable enhanced Central Processing Unit instruction sets (`/arch:AVX2`); and to explicitly target 64-bit x64 hardware.

This approach of interfacing with a DLL written in C++, and careful parallelization and compilation, outperformed

earlier versions of the module written entirely in Python considerably. Ultimately, this enables us to tackle larger sequences of observations with more distinct observations.

6 Methods for evaluating clusters and models

We next discuss methods which can aid in evaluating clusters and models for sequential data obtained from real-world processes. These methods have to account for the fact that, since we are dealing with real-world nonsynthetic data, we do not know the true process which generated the data. In particular, we do not have access to a ground-truth clustering.

6.1 Performance on a downstream task

One reason to cluster observations of sequential data, is that the clusters provide a tool for dimensionality reduction in subsequent statistical analyses or optimization procedures. For instance, the running time of a numerical method which aims to execute some computational task on a sequence of observations may grow considerably with the number of distinct observations n . In such a case it is clear that one has to reduce n or otherwise use a different algorithm. Reducing n can furthermore reduce issues associated with overfitting, and aid in human interpretability.

On the other hand, clustering naturally removes some information from the dataset. Thus, in a good clustering, the data should retain as much useful information as is possible. The meaning of “amount of useful information” is here ambiguous and depends on the context.

There are cases, however, in which the amount of useful information can be made concrete. Suppose for instance that one has a measure of quality $Q_{\text{pre-reduction}} := Q(T)$, evaluating performance of a downstream task $T := T(X_{1:\ell})$ applied to the sequence of observations. For example, if the algorithm is estimating parameters of some parametric model, then $Q_{\text{pre-reduction}}$ may be the accuracy of prediction on a validation dataset. One can now use this measure of quality $Q_{\text{pre-reduction}}$ as a proxy for the notion of useful information in a clustering. Given a clustering $\sigma_n : [n] \rightarrow [K]$ that reduces the number of distinct observations to some $1 \leq K \ll n$, one can apply the numerical solution method to obtain a solution $\tilde{T} := T(\sigma_n(X_{1:\ell}))$. The quantity $Q_{\text{reduced}} := Q(\tilde{T})$ then allows us to determine the quality of the clusters.

Using Q to determine the amount of useful information in clusters can help compare the quality of a number of different clusters which are output by different clustering algorithms. It can also happen that $Q_{\text{reduced}} > Q_{\text{pre-reduction}}$ due to the reduction of noise within the sequence of grouped observations. In fact, this effect may occur regardless of whether the task is numerically challenging. In the scenario where the task is numerically challenging, then the dimension reduction (from n to K) by the map σ_n still means that we can expect improved performance over methods that do not cluster data when fixing the computational budget.

In the following Sections 6.2 to 6.4 we discuss methods which can also reveal whether the BMC model is appropriate, and do not require some data-specific measure of quality.

6.2 Model selection with validation data

Section 6.1 mentioned that prediction of a validation dataset can serve as a measure of quality Q . We now expand on this idea.

6.2.1 Rescaled log-likelihood ratio

Assume we observe sequential data $X_{1:\ell}$ generated by some ground-truth probability distribution \mathbb{T} on $[n]^{\ell+1}$. The law \mathbb{T} can in principle be arbitrarily complex; for example, the Markov property need not be satisfied. Note that, for nonsynthetic data, we typically do not have access to the ground-truth \mathbb{T} . Suppose however that we do have two candidate models \mathbb{P} and \mathbb{Q} which are also defined on $[n]^{\ell+1}$. We then want to determine whether \mathbb{P} or \mathbb{Q} is a better model based on the observed sequential data $X_{1:\ell}$.

For this purpose, we consider a log-likelihood ratio. Namely, given $x_{1:\ell} \in [n]^{\ell+1}$, consider the quantity

$$\hat{D}(x_{1:\ell}; \mathbb{P}, \mathbb{Q}) := \frac{1}{\ell} \ln \frac{\mathbb{P}[X_{1:\ell} = x_{1:\ell}]}{\mathbb{Q}[X_{1:\ell} = x_{1:\ell}]} \quad (13)$$

and its expectation

$$D(\mathbb{T}; \mathbb{P}, \mathbb{Q}) := \mathbb{E}_{\mathbb{T}}[\hat{D}(X_{1:\ell}; \mathbb{P}, \mathbb{Q})]. \quad (14)$$

Then, if $D(\mathbb{T}; \mathbb{P}, \mathbb{Q}) > 0$ we consider \mathbb{P} to be a better approximation of the ground truth \mathbb{T} and if $D(\mathbb{T}; \mathbb{P}, \mathbb{Q}) < 0$ we consider \mathbb{Q} to be a better approximation. In practice we can not compute the expectation $\mathbb{E}_{\mathbb{T}}$ and instead consider the sign of the empirical estimator $\hat{D}(X_{1:\ell}; \mathbb{P}, \mathbb{Q})$.

In our experiments it is often the case that \mathbb{P} and \mathbb{Q} are MCs on $[n]$ whose transition matrices $P, Q \in [0, 1]^{n \times n}$ are known. In this case one can alternatively express (13) as

$$\hat{D}(x_{1:\ell}; \mathbb{P}, \mathbb{Q}) = \frac{1}{\ell} \sum_{t=1}^{\ell} \ln \frac{P_{x_t, x_{t+1}}}{Q_{x_t, x_{t+1}}}. \quad (15)$$

Confidence bounds for the estimation of $D(\mathbb{T}; \mathbb{P}, \mathbb{Q})$ by $\hat{D}(X_{1:\ell}; \mathbb{P}, \mathbb{Q})$ in this MC-setting are provided in Supplement 13. It is there additionally assumed that \mathbb{T} is a, possibly time-inhomogeneous, MC whose mixing time is known.

6.2.2 Information-theoretic interpretation for $D(\mathbb{T}; \mathbb{P}, \mathbb{Q})$

Let us briefly note that (14) has an information-theoretic interpretation. Namely, observe that

$$D(\mathbb{T}; \mathbb{P}, \mathbb{Q}) = \frac{1}{\ell} (\text{KL}(\mathbb{T}; \mathbb{Q}) - \text{KL}(\mathbb{T}; \mathbb{P})) \quad (16)$$

where KL denotes the Kullback–Leibler (KL) divergence

$$\text{KL}(\mathbb{T}; \mathbb{P}) := \mathbb{E}_{Z_{1:\ell} \sim \mathbb{T}} \left[\ln \left(\frac{\mathbb{T}(X_{1:\ell} = Z_{1:\ell})}{\mathbb{P}(X_{1:\ell} = Z_{1:\ell})} \right) \right]. \quad (17)$$

One can interpret the quantity $\text{KL}(\mathbb{T}; \mathbb{P})$ as the expected amount of discriminatory information revealing that \mathbb{P} is not quite the ground-truth probability distribution underlying the sample path $X_{1:\ell}$; see [45]. In many cases, such as when the ground-truth \mathbb{T} is an ergodic Markov chain, it further holds that (17) grows linearly in terms of amount of data ℓ .

Correspondingly, by (16), one can view $D(\mathbb{T}; \mathbb{P}, \mathbb{Q})$ as measuring the rate of growth for discriminatory information revealing that \mathbb{P} is a better approximation for the ground truth \mathbb{T} than \mathbb{Q} . To emphasize this perspective we will refer to $\hat{D}(X_{1:\ell}; \mathbb{P}, \mathbb{Q})$ as the *KL divergence rate difference estimator*.

6.2.3 Estimation when the models are inferred from the data

Our experiments routinely determine two different candidate models that we wish to compare, from the same one sample

sequence available to us. Let us emphasize this fact by referring to these candidate models as

$$\hat{\mathbb{P}}^{X_{1:\ell}} \quad \text{and} \quad \hat{\mathbb{Q}}^{X_{1:\ell}}. \quad (18)$$

Observe now that these two candidate models are a function of the observed data $X_{1:\ell}$. Substituting (18) into (13) could consequently result in a biased estimator and typically favor models with many parameters; the “optimal” model would be the degenerate probability distribution assigning probability 1 to the observed $X_{1:\ell}$.

To reduce the bias, we will use a holdout method. Specifically, we will split the trajectory into two parts: the first half $X_{1:\lfloor \ell/2 \rfloor}$ will be used for training, and the second half $X_{\lfloor \ell/2 \rfloor + 1:\ell}$ for validation. The quantity

$$\hat{D}(X_{\lfloor \ell/2 \rfloor + 1:\ell}; \hat{\mathbb{P}}^{X_{1:\lfloor \ell/2 \rfloor}}, \hat{\mathbb{Q}}^{X_{1:\lfloor \ell/2 \rfloor}}) \quad (19)$$

will likely still be a biased estimator of $D(\mathbb{T}; \mathbb{P}, \mathbb{Q})$ due to the dependence in the sequential data. The amount of bias should be however be significantly reduced when compared to the estimator obtained when substituting (18) into (13).

Note that (19) can be viewed as a measure of quality in the language of Section 6.1. Eq. (19) namely compares whether $\hat{\mathbb{P}}^{X_{1:\lfloor \ell/2 \rfloor}}$ or $\hat{\mathbb{Q}}^{X_{1:\lfloor \ell/2 \rfloor}}$ better predicted the validation data.

6.3 Model selection with only training data

As discussed in Section 6.2, the KL-divergence rates can provide a good rule-of-thumb for assessing what models are most interesting but are biased towards models with more parameters if one does not split the data into training and validation data. Splitting the data is however sometimes undesirable. Namely, if the data is sparse, the estimated models will become even less accurate. In order to overcome this issue, we will use information criteria that compensate the bias incurred and use it to assess the order of the cluster process.

6.3.1 Problem setting: order of a BMC

Suppose that a sequence $X_{1:\ell}$ was in fact generated by some r th-order BMC, but that the order $r \in \{0, 1, \dots\}$ is unknown. We will use techniques for model selection to try and determine r from the cluster sequence $Y_{1:\ell} = \sigma_n(X_{1:\ell})$.

There are two reasons for using $Y_{1:\ell}$ instead of $X_{1:\ell}$. First, the parametric models for higher order MCs without clusters have a comparable number of free parameters as the sequence length ℓ itself, so estimators for the order will behave poorly. If we look at the cluster chain instead, the number of degrees of freedom will depend on the cluster number K instead of the number of states n , and fortunately $K \ll n$. Secondly, we can also study the robustness of the model selection procedure depending on the clustering algorithm.

6.3.2 Order selection by minimizing an information criterion

The parameter that determines the r th-order BMC model for $Y_{1:\ell}$ is a transition matrix Q^r ; recall (7). Note here that the chain $Y_{1:\ell-r}^r$ will be constructed from the chain of clusters $Y_{1:\ell} = \sigma_n(X_{1:\ell})$ for a fixed cluster assignment σ_n .

To estimate Q^r one can consider the log-likelihood

$$\mathcal{L}(Y_{1:\ell} \mid Q^r) := \sum_{t=r}^{\ell-r-1} \ln Q_{Y_{t-r+1:t}, Y_{t+1}}^r. \quad (20)$$

The maximum-likelihood estimator associated with (20) is namely given by

$$(\hat{Q}^{r,\text{MLE}})_{i^r,j} := \begin{cases} \frac{\sum_{t=r}^{\ell-r-1} \mathbf{1}[Y_{t-r+1:t} = i^r, Y_{t+1} = j]}{\sum_{t=r}^{\ell-r-1} \mathbf{1}[Y_{t-r+1:t} = i^r]} & \text{if } \sum_{t=r}^{\ell-r-1} \mathbf{1}[Y_{t-r+1:t} = i^r] > 0, \\ 0 & \text{otherwise.} \end{cases} \quad (21)$$

Here i^r, j run over all possible sequences in $[K]^r$ and $[K]$ respectively. We denote $\hat{Q}^{r,\text{MLE}}$ for the law of an r th-order MC with K states and transition matrix $\hat{Q}^{r,\text{MLE}}$.

To determine what order r is the true underlying order of the data one would like to compare $\hat{Q}^{r,\text{MLE}}$ and $\hat{Q}^{s,\text{MLE}}$ for some $s \neq r$. As has been remarked in Section 3.2, using (13) for this purpose would give a biased estimator. Problems with bias in model selection are well-known in the statistics literature and to avoid this issue, the so-called *information criteria* were developed [42], [43], [44], [46], where to a log-likelihood a penalty term is added to correct the bias.

In our setting we need a penalty term that is sensitive to sparse data and is also consistent. For this purpose, we have chosen the Consistent Akaike Information Criterion (CAIC) [43]: for model $\hat{Q}^{r,\text{MLE}}$,

$$\text{CAIC}(\hat{Q}^{r,\text{MLE}}) := -2 \ln(\mathcal{L}(Y_{1:\ell} | \hat{Q}^{r,\text{MLE}})) + 2\text{DF}(K, r)(1 + \ln(\ell - r)). \quad (22)$$

Here, $\text{DF}(K, r)$ the degrees of freedom in an r th-order MC constrained to have fixed parameters K and r . Specifically,

$$\text{DF}(K, r) = K^r(K - 1) \quad (23)$$

where the factor $(K - 1)$ is due to the fact that the rows of Q^r are constrained to add up to one. We will utilize the CAIC to select the right order as follows. From the collection of models $\hat{Q}^{0,\text{MLE}}, \hat{Q}^{1,\text{MLE}}, \hat{Q}^{2,\text{MLE}}, \dots$, we may determine the order r^{CAIC} that minimizes the CAIC:

$$r^{\text{CAIC}} := \operatorname{argmin}_{r \in \{0,1,2,\dots\}} \text{CAIC}(\hat{Q}^{r,\text{MLE}}). \quad (24)$$

Note that lower-dimensional models are favored since the degrees of freedom $\text{DF}(K, r)$, and thus the penalty terms in (22), increase exponentially in K, r .

In order to evaluate how robust the CAIC criterion is, we will estimate the over- and underfit error probabilities with error models and draw conclusions on the selected orders.

6.4 The shape of spectral noise for identification of alternative models

The methods in Sections 6.1 to 6.2 allow us to compare a BMC to alternative models. The selection of a good alternative can however be difficult when a more complex model than a BMC is desirable. The method described here can aid in the selection of an alternative model.

The method is based on a result from [5] which describes the histogram of the singular values of \hat{N} in the asymptotic regime $n \rightarrow \infty$ under the condition that $\ell = \Theta(n^2)$. The results in [6] can further be interpreted as the statement that the K nonzero singular values of $\mathbb{E}[\hat{N}]$ correspond to the K largest singular values of \hat{N} . In other words, all singular values except these leading few may be interpreted as being due to the noise $\hat{N} - \mathbb{E}[\hat{N}]$. The histogram of the nonleading singular values may thus be interpreted as the *shape of the spectral noise*.

These results and their interpretation can guide the selection of a good model. One can namely identify clusters in the data and visually compare the associated BMC-prediction with the observed histogram. If there is a good match, then this may indicate that a BMC suits the data well. If there is a discrepancy, then the nature of the discrepancy can be informative of the properties that the alternative model should have. It will for instance be shown in Supplement 14.4 that a long tail can sometimes be explained using a heavy-tailed perturbation.

We have, however, found that a strongly inhomogeneous equilibrium distribution in the data can dominate the spectral noise in \hat{N} . So long as the clustering respects the equilibrium distribution it then follows that the observations will indeed resemble the theory. This is an issue since it follows that, in the case of an inhomogeneous equilibrium distribution, the spectral noise of \hat{N} may not be particularly informative. In such a case one can consider a different random matrix.

The *empirical normalized Laplacian* \hat{L} associated to the observation sequence is element-wise given by

$$\hat{L}_{ij} := \begin{cases} \frac{\hat{N}_{ij}}{\sqrt{\sum_{k=1}^n \hat{N}_{ik}} \sqrt{\sum_{k=1}^n \hat{N}_{kj}}} & \text{if } \hat{N}_{ij} \neq 0, \\ 0 & \text{otherwise.} \end{cases} \quad (25)$$

We argue in Supplement 14.3 that the variance of the entries of \hat{L} is approximately independent of the equilibrium distribution. Consequently, we expect that the spectral noise of \hat{L} will not be dominated by a possibly inhomogeneous equilibrium distribution. A proposition describing the limiting histogram of singular values is proved in Supplement 14.3. The precise statement is technical but a summary may be found in Proposition 1.

Proposition 1. *Let $X_{1:\ell}$ be a sample path of a BMC. If $\ell = \Theta(n^2)$, then for almost every $a, b \in \mathbb{R}$ the fraction of singular values in $[a, b]$, i.e., $n^{-1} \#\{i : s_i(\sqrt{n}\hat{L}) \in [a, b]\}$ converges in probability as $n \rightarrow \infty$. The limit may be computed explicitly in terms of the parameters of the BMC.*

With Proposition 1, we can characterize the spectral noise of \hat{L} in a BMC and use the spectrum as a tool for data exploration, expectedly even in the presence of an inhomogeneous equilibrium distribution.

7 Data sets and preprocessing

We are going to apply the clustering algorithm described in Section 5 to different data sets. First, however, we will introduce the data sets, specify the sequence $X_{1:\ell}$, and describe any preprocessing that we have conducted. The results of clustering can be found in Section 8.

7.1 Sequence of codons in DNA

We will consider the OCA2 gene in human DNA, and source the data from [47]. The OCA2 gene provides instructions for making a protein located in melanocytes, which are specialized cells that produce a pigment called melanin. It must be noted that the clustering algorithms can be applied to any gene. We expect similar results in other human DNA; the OCA2 gene serves here merely as an example.

A typical string of DNA can be viewed as a sequence composed of four possible nucleotides denoted by A, T, C and

G. These nucleotides are moreover naturally clustered together in three-letter words called *codons* which are processed in protein synthesis within a cell. For instance, the codon ACG corresponds to the addition of the amino acid *threonine* as the next building block of a protein. From a sequence of nucleotides such as

TTT GTA GTT AGA TCT CCT CTA TCC *et cetera*,

we thus identify the sequence of codons

$$X_1 = \text{TTT} \rightarrow \dots \rightarrow X_8 = \text{TCC} \rightarrow \textit{et cetera}.$$

The empirical frequency matrix in (10) is calculated, and found to have $\ell = 16 \times 10^4$ transitions and a state space of size $n = 64$.

7.2 Sequence of words in texts

A cleaned corpus, based on the Wikipedia datadump of October 2013, was downloaded from [48]. This cleaned corpus filters on popularity to exclude a large amount of robot-generated pages. Further preprocessing was standard: we removed all punctuation and numbers, reduced all words to lower case and reduced all words to a root word with the Natural Languages Toolkit’s `PorterStemmer.stem()` [49, Section 3.6]. The 100 most visited words were pruned from the data as well as all words with fewer than 1000 visits. This results in a vocabulary of $n = 16994$ words. For example, a paragraph such as

Clustering observations can be very useful!

is converted into the sequence

$$X_1 = \text{cluster} \rightarrow X_2 = \text{observ} \rightarrow \dots \rightarrow X_6 = \text{use}.$$

Each s th Wikipedia page results in a sequence $X_{1:\ell^s}$ say that is relatively short when compared to n . The corresponding frequency matrix \hat{N}^s , recall (10), is consequently sparse. We therefore compute and work instead with

$$\hat{N} := \sum_s \hat{N}^s. \quad (26)$$

The diagonal of the *summed empirical frequency matrix* in (26) is set to zero. Self transitions are namely common and not particularly informative for the purposes of clustering. The remaining total number of transitions is found to be $\ell \approx 2 \cdot 10^8$.

7.3 Sequence of animal positional data

GPS animal movement data, at its core, is a set $Y = \{y_1, \dots, y_n\}$ of observation tuples $y_i = (y_{i1}, y_{i2}, y_{i3})$, in which the elements y_{i1}, y_{i2}, y_{i3} correspond to a latitude, a longitude, and a timestamp, respectively. We presume that the latitude and longitude are measured in decimal degrees.

If we were to assume that every distinct GPS coordinate (y_{i1}, y_{i2}) of the observation tuple corresponds to a distinct state of a BMC, then the clustering problem will turn out to be infeasible. The reason is that there would be nearly as many states as there are observations. We must therefore combine GPS coordinates into states during preprocessing. Specifically, we divide the two-dimensional region in which all GPS points lie (a manifold) into a two-dimensional grid of squares with width x km. The number x is to be chosen according to the considered data, leading to a desired amount of states. Details on this step can be found in Supplement 15.2.

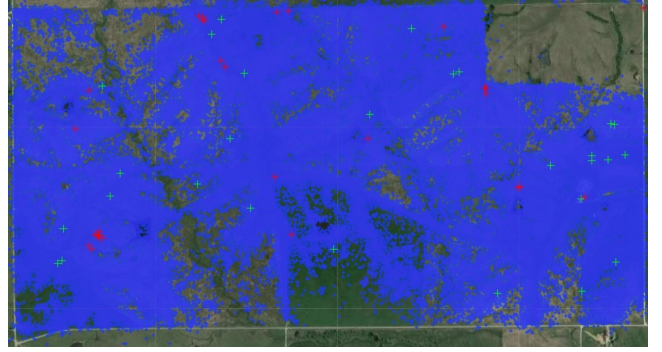


Fig. 3. A screenshot from movebank displaying the raw GPS data.

For this investigation we (arbitrarily) choose data from the “Dunn Ranch Bison Tracking Project,” freely accessible through [50, #8019591]. The data is displayed in Figure 3. The area is approximately rectangular with length $l \approx 3.2$ km and width $w \approx 1.7$ km. For example, the tracking data of one animal starts with the following observations:

$$\begin{aligned} &(40.4749, -94.1129, 21:00), (40.4748, -94.1130, 21:15), \\ &(40.4749, -94.1129, 21:30), (40.4751, -94.1130, 21:45), \\ &(40.4749, -94.1130, 22:00), (40.4749, -94.1129, 22:15), \\ &\quad \textit{et cetera}. \end{aligned} \quad (27)$$

These observations for this particular animal were registered on October 24, 2012. The study includes movement data from 24 animals, and we concatenate all of the movement data to create a single long observation sequence.

Some registered GPS coordinates are outside the piece of land that we consider. This was most likely caused by some malfunction of the GPS tracking device. We therefore exclude all observation tuples y_i for which $y_{i1} \notin (40.47, 40.4861)$ or $y_{i2} \notin (-94.1183, -94.079121)$. After this pre-processing, the single observation sequence that we obtain is of length 337003. After preprocessing with grid size $x = 0.04$ km (chosen by *ad hoc* parameter tuning), we identify the start of the sequence:

$$\begin{aligned} X_1 &= \text{Bin 0} \rightarrow X_2 = \text{Bin 1} \rightarrow X_3 = \text{Bin 0} \\ &\rightarrow X_4 = \text{Bin 0} \rightarrow X_5 = \text{Bin 0} \rightarrow X_6 = \text{Bin 0} \rightarrow \textit{et cetera}. \end{aligned}$$

We finally eliminated self-jumps such that resting animals do not disturb our findings. From this sequence of states, the empirical frequency matrix defined in (10) is calculated. Ultimately, we were working with $n = 3155$ states and an observation sequence of length $\ell = 193134$ when the self-jumps were excluded. This gives us quite a short path; $\ell/n^2 \approx 0.0194$.

7.4 Sequence of companies with the highest daily return

Using Alpha Vantage’s API [51], we downloaded 20 years of daily pricing data for every company within the S&P500 index. The S&P500 index is a gauge for the performance of large market capitalization U.S. equities. The index includes 500 companies and covers approximately 80% of available market capitalization. The top constituents by index weight currently include, for example, AAPL (Apple), MSFT (Microsoft), AMZN (Amazon), TSLA (Tesla), and GOOGL (Alphabet).

The pricing data of the constituents turned out to not span the same one time range. We therefore sorted the pricing data

files of the different constituents by file size and kept the data for the 300 companies with the most complete data. A list of these constituents can be found in Supplement 16.3. Next, we determined for each constituent $i \in [300]$ when the first data entry happened, t_-^i , and when the last data entry happened, t_+^i . We finally restricted our analysis to the time range

$$\max_{i \in [300]} t_-^i =: t_0, t_0 + 1, \dots, t_0 + \ell := \min_{i \in [300]} t_+^i \quad (28)$$

for these 300 companies. It turned out that $t_0 \equiv 2001-07-26$ and $t_0 + \ell \equiv 2021-10-22$. Days without any pricing data were ignored, which include the weekends when the stock market is closed. Ultimately, for every remaining day with some pricing data, the data was in fact complete: we have all daily opening and closing prices for each of these 300 constituents.

For $t = t_0, \dots, t_0 + \ell$, let O_t^i denote the opening price of company i 's stock on day t and C_t^i the closing price of company i 's stock on day t . We then considered the *daily return* of company i 's stock on day t ,

$$R_t^i = \frac{C_t^i}{O_t^i} - 1 \quad \text{and let} \quad X_t \in \arg \max_{i \in [300]} R_t^i \quad (29)$$

be a company with the highest daily return on day t . Ties are broken uniformly at random. For example, the preprocessing output's start looks like:

On 2001-07-26, maximizer ADI had return 0.12517.
 On 2001-07-27, maximizer AES had return 0.08905.
 On 2001-07-30, maximizer PVH had return 0.04478.
 On 2001-07-31, maximizer HUM had return 0.09852.
 On 2001-08-01, maximizer NTAP had return 0.15665.
Et cetera.

so that the sequence of observations starts with

$$\begin{aligned} X_{t_0} &= \text{ADI}, X_{t_0+1} = \text{AES}, X_{t_0+2} = \text{PVH}, \\ X_{t_0+3} &= \text{HUM}, X_{t_0+4} = \text{NTAP}, \textit{et cetera}. \end{aligned} \quad (30)$$

We again eliminate self-jumps, this time to reduce the effect of profitable runs by companies that temporarily dominated the market. That is, we remove any consecutive appearance of a single constituent in the sequence. Note that this preprocessing only gives us one sequence, that is furthermore relatively short ($\ell/n^2 \approx 0.027$). Finally, we calculate the empirical frequency matrix in (10) and proceed with the clustering algorithm.

8 Detected clusters within the data

In this section, we evaluate how well the BMC model can approximate the structure of the different sequential data introduced in Section 7 and if it can yield useful insights.

8.1 Sequence of codons in DNA

We consider the sequence of codons occurring in the gene OCA2 in human DNA. Clustering on this sequence extracts an interesting pattern displayed in Figure 4(a). The detected clusters were:

$\mathcal{V}_1 = \text{AAA, AAG, TGT, AGT, CCT, TCT, ACT, CAG, ATT, ATG, CAT, TAT, AAT, TTG, CTT, TGA, CTG, CAA, TGG, ATA, TTA, AGG, TAA, ACA, TCA, CCA, AGA}$
 $\mathcal{V}_2 = \text{CAC, GCC, CCC, TCC, ACC, GTC, CTC, TTC, ATC, TGC, AGC, TAC, AAC, GGC, TAG, CTA, GAC}$
 $\mathcal{V}_3 = \text{GTG, GAG, GGT, GCA, GAA, GTA, GGA, GAT, GGG, GTT, GCT}$

$\mathcal{V}_4 = \text{CGA, CGC, ACG, TCG, CCG, GCG, CGT, CGG}$
 $\mathcal{V}_5 = \text{TTT}$

8.1.1 Possible detection of codon-pair bias

We observe that all rows and columns associated with the second-to-last community \mathcal{V}_4 have low density. This means that community \mathcal{V}_4 has a small equilibrium distribution. More interesting is the low-density block in the rows and columns corresponding to the transitions from the second community \mathcal{V}_2 to the third community \mathcal{V}_3 . It appears we have rediscovered a phenomenon known as *codon-pair bias* in biology [52], [53], [54]. A brief examination of biology literature suggests that there is a link between codon-pair bias and gene expression, which has been used to engineer weakened viruses which could potentially be used as a vaccine [55], [56], [53].

There is some evidence that codon-pair bias is nothing more than a consequence of *dinucleotide bias* [54]. Here, the term dinucleotide bias refers to the fact that the two-letter pair CG is only used infrequently regardless of its position. This dinucleotide bias can also explain the clusters observed in Figure 4(a). Indeed, inspection of the clusters $\mathcal{V}_1, \dots, \mathcal{V}_5$ reveals that nearly all codons in \mathcal{V}_2 end with the nucleotide C whereas all codons in community \mathcal{V}_3 begin with nucleotide G. There are a few exceptions, namely the codons TAG and CTA in \mathcal{V}_2 , but visual inspection of the matrix \hat{N} seems to suggest that these two codons may have been misclassified. Thus, transitions from \mathcal{V}_2 to \mathcal{V}_3 would give rise to the two nucleotides CG on the interface. Also remark that the two leftmost vertical low-density streaks in the block associated with \mathcal{V}_2 corresponds to the codons GCC and GTC which simultaneously begin with a G and end with a C. Finally, all codons in community \mathcal{V}_4 contain the two nucleotides CG. It thus appears that all low-density regions in the figure could be explained as being due to dinucleotide bias. We refer to [57] and the references therein for further discussions concerning codon-pair bias, dinucleotide bias and their applications.

8.1.2 Comparing the histogram of singular values to the limiting distribution of singular values of the inferred BMC

It appears from the reasonable clusters in Figure 4(a) that a BMC could be an appropriate model for this dataset. Let us now additionally verify whether the shape of the spectral noise is consistent with a BMC. Note that the matrices \hat{N} and \hat{L} are only 64×64 . Consequently, they only have 64 singular values. To get a clearer picture we split the observation sequence into ten equally sized pieces and for each subpath we compute the singular values. The averaged histogram over these ten observations is compared to the theoretical BMC-prediction associated to the clusters in Figure 4(b).

We observe a good match between the theory and the bulk of the distribution for both \hat{N} and \hat{L} . Particularly interesting is that the peak near zero and the triangular tail in the interval [4, 5]. The theoretical there matches the observed distribution for \hat{N}/\sqrt{n} . Such features would not be predicted in a simpler model without communities such as a matrix with i.i.d. entries. One would then instead expect a quarter-circular law whose density is proportional to $\mathbf{1}[x \in (0, c)]\sqrt{c^2 - x^2}$ for some constant $c > 0$. This quarter-circular law is observed in the empirical Laplacian \hat{L} suggesting that the main feature in the spectral noise of \hat{N} is due to the equilibrium distribution. There are also some rescaled singular values which escape the support

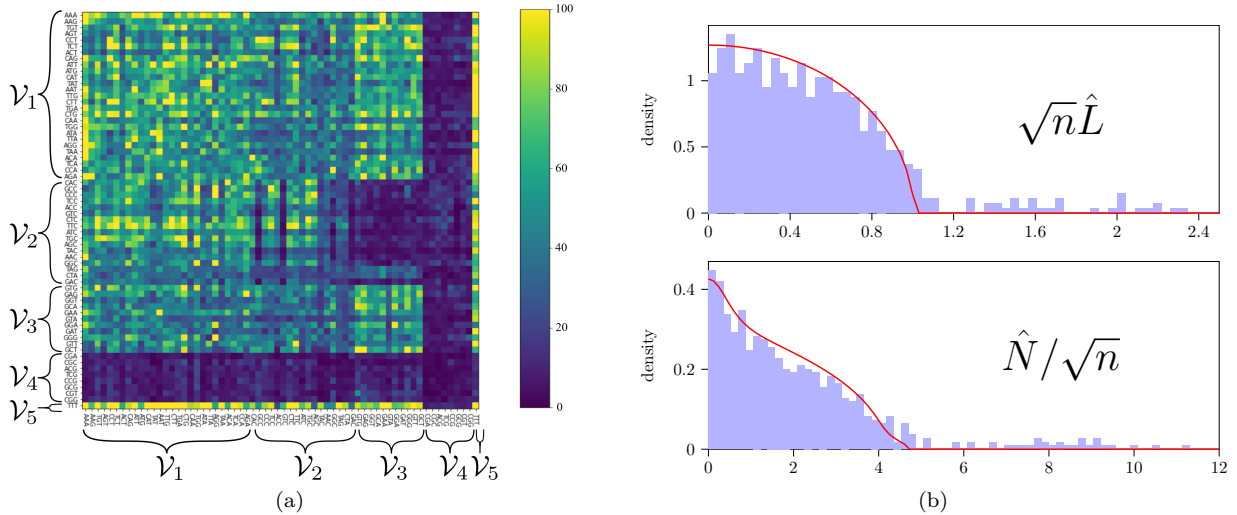


Fig. 4. (a) The frequency matrix \hat{N} when the codons are sorted by the five detected clusters. (b) Average density-based histogram of singular values for $\sqrt{n}\hat{L}$ and \hat{N}/\sqrt{n} for the DNA sequential data in blue bars and the theoretical predictions associated with the improved clustering as the red line. Not displayed is that each observation of \hat{N}/\sqrt{n} also has a single singular value near 40 and each observation of $\sqrt{n}\hat{L}$ has a single singular value near 8. These extremal singular values are considered to be part of the signal, and consequently not relevant for measuring the spectral noise.

of the limiting singular value distribution. These are most likely associated to the signal $\mathbb{E}[\hat{N}]$ and should consequently not be viewed as a part of the spectral noise.

8.1.3 Conclusion

It appears that the clustering algorithm was able to detect the phenomena of dinucleotide bias in DNA. The spectral noise is also consistent with that in a BMC. Moreover, a simpler model generating a random matrix with independent and identically distributed entries would not have sufficed to make the prediction associated to \hat{N} 's distribution of singular values.

8.2 Sequence of words on Wikipedia

We consider the sequence of words obtained after the pre-processing described in Section 7. The clustering algorithm discussed in Section 5 was executed for $K = 50, 100, 200, 400$ clusters, both with and without the improvement algorithm. Ten improvement iterations were done whenever we also used the improvement algorithm. A complete list of the clusters for $K = 200$ with improvement may be found in Supplement 16.2.

8.2.1 Subjective evaluation

At a first glance, the clusters that the clustering algorithm determines appear to be good. For instance, a small cluster with six elements has a distinctly football-related theme: \mathcal{V}_{125} contains the words *champion*, *cup*, *premier*, *coach*, *football* and *championship*. The medium-sized clusters \mathcal{V}_{50} , \mathcal{V}_{51} , and \mathcal{V}_{52} respectively contain words related to public professions, units, and warfare. That is, \mathcal{V}_{50} includes stemmed words such as *founder*, *deputi*, *formeli*, *mayor*, *bishop*, *meanwhil*, *successor*, \mathcal{V}_{51} includes *tonn*, *usd*, *capita*, *lb*, and \mathcal{V}_{52} includes *cavalri*, *jet*, *helicopt*, *rifl*, *warfar*, *battalion*, and *raid*. The second-largest cluster \mathcal{V}_2 predominantly contains names; these include *alexandr*, *albrecht*, *gideon*, and *jarrett*.

We further observe that the improvement algorithm yields more balanced clusters: before the improvement algorithm the largest three clusters have size 9192, 1279 and 1126 respectively while after improvement the sizes are 2848, 1943 and 1600.

8.2.2 Performance on a downstream task

To evaluate the quality of the clusters more objectively, we investigate the performance achieved on a downstream task as discussed in Section 6. We specifically consider the accuracy achieved by a document classification algorithm.

The goal in document classification is to predict the label $l(d)$ of a document d given some training dataset $\{(d', l(d'))\}$. The document datasets that we investigate are described in Supplement 16.2.1. For instance, the AG News dataset contains news articles with four possible labels: *World*, *Sports*, *Business*, and *Sci/Tech*.

Given a clustering, one can translate each document into an K -dimensional vector by counting the number of occurrences of each cluster in the document; see Supplement 15.1. Thereafter, a logistic regression model is trained to learn a mapping from the K -dimensional vectors to the labels. Aside from spectral and improvement clusters we also consider a random clustering in which every word was assigned a cluster uniformly at random. There were some datasets in which neither spectral nor improvement clustering significantly outperformed the random clustering. We consider these tests inconclusive, but still report them in Table 4 for completeness. The performance on the remaining datasets is displayed in Table 1.

Observe that improvement clustering typically outperforms plain spectral clustering. Further note that in the *AG News*, *Yahoo!* and *Wiki* datasets the performance increases with the dimensionality. The gain in performance from spectral and improvement clustering as opposed to random clustering is there comparable with an increase of dimensionality by a factor 4. On the other hand, for *Books* and *CMU* it appears that the performance decreases with the dimensionality although this pattern is less clear. A possible explanation is that *Books* and *CMU* have less training data so that overfitting may occur when the dimensionality is large.

K	Algorithm	AG News	Yahoo!	Wiki	Book	CMU
50	Random	48.3%	27.4%	56.9%	31.0%	67.4%
50	Spectral	66.0%	39.8%	71.1%	44.4%	69.5%
50	Improved	68.5%	40.1%	71.5%	44.7%	71.8%
100	Random	55.5%	33.3%	68.4%	30.0%	67.4%
100	Spectral	72.7%	47.2%	81.6%	45.2%	70.0%
100	Improved	76.8%	49.0%	80.1%	46.3%	70.7%
200	Random	64.0%	41.7%	80.8%	28.2%	66.8%
200	Spectral	78.2%	51.7%	85.6%	44.4%	68.7%
200	Improved	80.7%	54.7%	86.5%	43.4%	69.0%
400	Random	72.8%	49.4%	87.8%	28.9%	66.8%
400	Spectral	81.5%	56.3%	88.0%	42.1%	67.9%
400	Improved	83.1%	58.6%	89.0%	44.4%	68.4%

TABLE 1

Performance of clustering before and after improvement as measured by accuracy in the downstream task of document classification as compared to a random clustering. Bold added for the best-performing method.

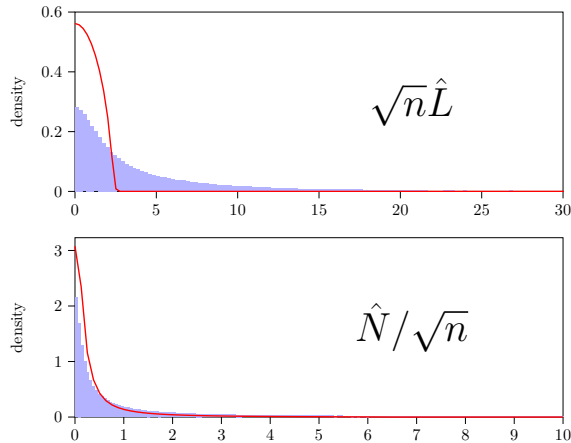


Fig. 5. Density-based histogram of singular values for $\sqrt{n}\hat{L}$ for the words sequential data in blue bars and the theoretical predictions associated with the improvement clustering with $K = 200$ as the red line. Not visible in this figure is that both empirical distributions have long tails. Still 9% of the singular values of \hat{N}/\sqrt{n} exceed 10 and 1% of the singular values of $\sqrt{n}\hat{L}$ exceed 30.

8.2.3 Comparing the histogram of singular values to the limiting distribution of singular values of the inferred BMC

One may be tempted to deduce from the reasonable clusters and the performance reported in Table 4 that the BMC is an appropriate model for this dataset. The structure in the spectral noise is however not as one would expect in a BMC. Consider Figure 5 for a comparison of the empirical singular value distribution with the theoretical predictions. Observe that there is a good match for \hat{N} but a discrepancy for \hat{L} .

The fact that \hat{N} yields a good match can be explained as being due to a strongly inhomogeneous equilibrium distribution from Zipf’s law. The empirical Laplacian \hat{L} removes this dominant effect after which it may be observed that the empirical distribution has a heavy tail which is not present in the BMC-based prediction. In Supplement 14.4 we demonstrate by a numerical example that the discrepancy which is observed in Figure 5 agrees precisely with the type of discrepancy which is observed for a heavy-tailed perturbation of the BMC. The fact that the entries of the matrices \hat{N} and \hat{L} are heavy-tailed may also be verified by direct inspection.

8.2.4 Conclusion

The clustering algorithm was able to detect clusters which we subjectively judge to be interesting. The performance on the downstream task of document classification further indicated that the improvement algorithm which is based on the BMC-assumption improved the quality of the clusters. The spectral noise indicated that there is some heavy-tailed component in the matrix which can not be accounted for in the BMC assumption. It is correspondingly conceivable that a different model could incorporate the heavy-tailed nature of the entries and extract even better clusters.

8.3 Animal movement data

We investigate now the GPS animal movement data from the *Dunn Ranch Bison Tracking Project*; recall Section 7.

8.3.1 Subjective evaluation

The results of the clustering algorithm are depicted in Figure 6. It is subjectively evident that the clusters give more insight than the scatter plot in Figure 3.

Observe that the clustering algorithm picks up on geographical features: all clusters are connected regions, except for the largest two clusters 1 (black dots) and cluster 2 (orange c ’s), however the individual components are connected. Clusters 1 and 2 contain the low degree states which explains their geographical spread. For the other clusters geographical boundaries are visible. For example, cluster 3 is bounded from below by creeks and cluster 4 lies between two creeks. On satellite imagery one can see a fence north of 7 and the part of 2 (orange c ’s) that is bordering 7 and in fact, the northern border of these two clusters follows that line.

We briefly want to address that the average rate of transitions within each cluster is 0.79. The transitions that are shown on the map are thus not representing the majority of transitions, but only the transitions between different clusters that occur with probability of at least 0.01. The cluster transitions matrix is given in Supplement 16.1.

We summarize the findings: regions where the animals stay or pass through are determined; barriers such as rivers, lakes and fences can be seen; and average movement patterns of the animals are deduced. This is actually surprising, because the clustering algorithm identifies states by numbers and does *not* use geographical information on the state labeling. The labels of the states are in fact arbitrary to the algorithm, states labeled e.g. 10 and 11 need not be close to each other geographically. We remark that geographically mixed clusters would have been a valid outcome of the algorithm. Instead, we see that the clustering algorithm clusters states in such a manner that their geographical positions correspond to connected regions with clear borders.

In short: the algorithm detects geographical features and movement patterns, and the algorithm does so based on the sequential data alone, i.e., it captures behavior of the animals.

8.3.2 Comparing the histogram of singular values to the limiting distribution of singular values of the inferred BMC

Figure 7 next compares the spectral noise of (10) and (25) to the theoretical predictions for BMCs (recall Proposition 2). Observe that with $K = 15$ clusters, the theoretical prediction captures the general shape of the distribution, but is inaccurate

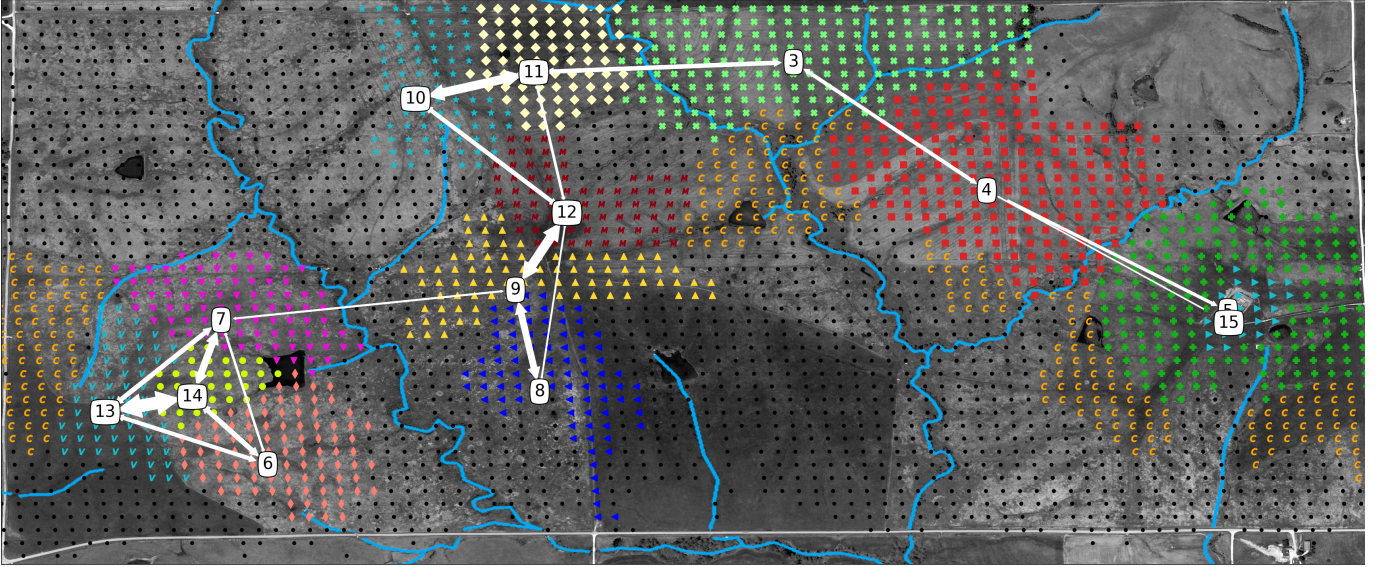


Fig. 6. The Dunn Ranch with highlighted water, on top of which the detected clusters are mapped. Additionally, the cluster centers are indicated with boxes containing the cluster number and edges between the boxes indicate the transitions between clusters with probability of at least 1%. Thicker arrows correspond to higher transition probabilities. Self-transitions and the clusters 1 and 2 are omitted, because they are non-informative.

for the smallest and largest singular values especially. With more clusters, $K = 100$, the theoretical prediction for the distribution of singular values is found to predict the distribution of singular values better across the entire range. The prediction however remains imperfect. The peak at zero is probably linked to the fact that there are many states with a low degree.

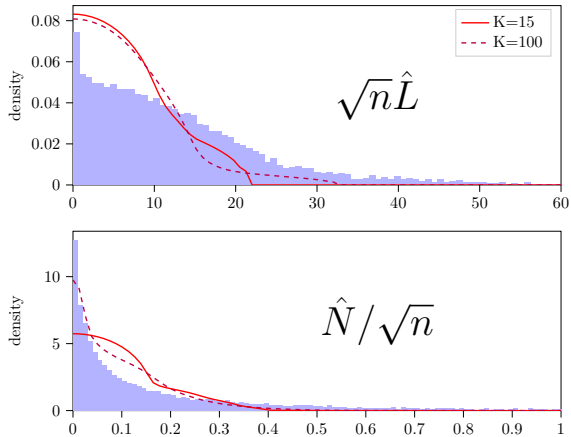


Fig. 7. Density-based histogram of singular values for $\sqrt{n}\hat{L}$ and \hat{N}/\sqrt{n} for the animal movement data in blue bars and the theoretical predictions associated with the improvement clustering with $K = 10$ as the red line and with $K = 100$ as the purple dashed line.

8.3.3 Conclusion

We conclude that a BMC is a useful model for describing animal movement data. In fact, surprisingly, the clustering algorithm manages to deduce underlying geographical information (such as regions, barriers, and movement patterns) from the mere time dependency within the observation sequence. Because of this visuo-spatial ability, the algorithm may have a potential use as a tool for spatial recognition.

At the same time however, we also conclude that a BMC does not describe the underlying complex process in its entirety.

For example, the distribution of singular values depicted in Figure 7 is not predicted perfectly. This is likely caused by the symmetry assumption between states within a BMC, which is at odds with the geographical structure of the data. Indeed, if we cut the region into more but smaller clusters and thus reduce the amount of symmetry within the BMC modeling the observation sequence, the BMC's prediction of the distribution of singular values improves.

8.4 Companies with the highest daily returns

We turn now to the last analyzed dataset: the sequence of companies with the highest daily returns. The analysis for this dataset was particularly delicate to conduct and we ultimately arrive at the conclusion that a 0th-order BMC could already be sufficient to explain the found clusters. This conclusion may appear disappointing; it namely means that the clusters may not encode any order-dependent dynamics of the process. It is however important for a practitioner to be able to arrive at this conclusion when appropriate. The fact that the evaluation methods from Section 6 are able to suggest a 0th-order BMC is correspondingly a good feature of the methods: the comparison method would not be informative in the alternative scenario where one always concludes in favor of the 1st-order BMC. The main goal of this section is hence to demonstrate how the methods of Section 6 can be used for the comparison of different models; even in a difficult, sparse, regime.

Let us note that there are two main reasons why this dataset is difficult to analyse. First, the data is sparse. It namely holds that $\ell/n^2 \approx 0.027$. The sparsity can also be observed by direct inspection of \hat{N} ; see Figure 12 in Supplement 16.3.3. This sparsity makes recovery of the clusters a hard problem, even if the data-generating-process is truly a BMC, and moreover makes evaluation of the found clusters more difficult since the associated confidence bounds are large. Second, it turns out that the data contains a strong 0th-order BMC component. This strong 0th-order component could potentially serve as a nuisance factor and could conceal a 1st-order BMC component

even if it exists. This second factor may explain why the animal movement data in Section 8.3 did not suffer from a difficult analysis despite it being even sparser; $\ell_{\text{animal}}/n_{\text{animal}}^2 \approx 0.0194$.

8.4.1 Subjective evaluation of the clusters

After some *ad hoc* experimentation, we fix $K = 3$.

The S&P500's factsheet labels every constituent with a sector. The sector breakdown within the dataset is shown in Table 5 in Supplement 16.3.1. We can use this labeling to obtain "fingerprints" of clusters, and to compare the labeling of the clustering algorithm against.

Such comparisons are plotted in Figure 8 for the three largest clusters. The black bars show the relative percentages of constituents in each sector within the clusters detected by the spectral algorithm followed by the cluster improvement algorithm. Observe the absence of most utilities constituents within the 2nd and 3rd cluster; more than twice as many are assigned to the 1st cluster than may be expected from a random assignment. Industrial and health care constituents are also mostly absent within the 3rd cluster. Similarly, note the negligible number of consumer discretionary constituents within the 1st cluster; most are assigned to the 2nd and 3rd cluster. Finally, consider that the 3rd cluster consists for 29% out of information technology constituents. These contents suggest that the clusters are not entirely random. The subsequent experimentation aims to determine what type of information has been encoded in the clusters.

As a subjective way to evaluate the meaning of the clusters, let us inspect the relative cluster sizes $\hat{\alpha}_k := \#\hat{V}_k/n$, cluster equilibrium distribution $\hat{\pi}$, and cluster transition matrix \hat{p} of the associated BMC:

$$\hat{\alpha}^T \approx \begin{pmatrix} 0.45 \\ 0.45 \\ 0.10 \end{pmatrix}, \quad \hat{\pi}^T \approx \begin{pmatrix} 0.49 \\ 0.10 \\ 0.41 \end{pmatrix}, \quad \hat{p} \approx \begin{pmatrix} 0.50 & 0.10 & 0.40 \\ 0.54 & 0.11 & 0.35 \\ 0.46 & 0.10 & 0.44 \end{pmatrix}.$$

Note that the rows of \hat{p} are close to but not quite equal; it namely holds that $\hat{p}_{kl} \approx \hat{\pi}_l$ for every k, l . This observation may suggest a strong 0th-order BMC component. One can however not immediately conclude that all the deviations from constant columns are due to noise: the data is sparse relative to n^2 but not when compared to $K^2 = 9$.

8.4.2 Comparing against alternative models

Recall that, using validation data, we can compare the performance of different models by the KL divergence rate difference estimator (19). Consider the following models:

- $\hat{\mathbb{P}}$: A 1st-order BMC with $m = 3$ clusters determined by the spectral algorithm followed by the improvement algorithm.
- $\hat{\mathbb{Q}}_1$: A 1st-order BMC with $m = 11$ clusters given by the constituents' sector labels.
- $\hat{\mathbb{Q}}_2$: A 1st-order BMC with $m = 3$ clusters, determined by the spectral algorithm.
- $\hat{\mathbb{Q}}_3$: A 0th-order BMC with $m = 3$ clusters, determined by sorting according the state's sample equilibrium distribution and determining clusters of equal probability mass.
- $\hat{\mathbb{Q}}_4$: A 0th-order BMC with $m = 3$ clusters, determined by the spectral algorithm followed by an improvement algorithm (appropriately modified for a 0th-order BMC).

One may also wonder about the relevancy of the number of parameters. By keeping the number of clusters fixed it namely

also follows that the 0th-degree models $\hat{\mathbb{Q}}_2, \hat{\mathbb{Q}}_3$ have fewer parameters than the 1st-degree models $\hat{\mathbb{P}}, \hat{\mathbb{Q}}_4$. To this end, consider for any positive integer $k \geq 1$ the following model:

$\hat{\mathbb{Q}}_{3,k}$: A 0th-order BMC with k clusters, determined by sorting according the state's sample equilibrium distribution and determining k clusters of equal equilibrium probability.

Note that the degrees of freedom $DF_1(n, K)$ within a 1st-order BMC constrained to have fixed parameters (n, K) equals $DF_1(n, K) = n + K(K - 1)$, whereas the degrees of freedom $DF_0(n, K)$ within a 0th-order BMC constrained to have fixed parameters (n, K) equals $DF_0(n, K) = n + K - 1$. The model $\hat{\mathbb{P}}$ therefore has $n + 6$ degrees of freedom whereas $\hat{\mathbb{Q}}_{3,k}$ has $n + k - 1$ degrees of freedom. In terms of number of degrees of freedom, $\hat{\mathbb{P}}$ is thus comparable to $\hat{\mathbb{Q}}_{3,7}$. Observe furthermore that $\hat{\mathbb{P}}$ allows for more inhomogeneity within the columns of the transition matrix and less in the rows, whereas $\hat{\mathbb{Q}}_{3,7}$ allows for no inhomogeneity within the columns but more in the rows.

Observe in Figure 9(a) that the difference in KL divergence rate on the validation data is positive when comparing $\hat{\mathbb{P}}$ against $\hat{\mathbb{Q}}_1, \hat{\mathbb{Q}}_2$, barely positive when comparing against $\hat{\mathbb{Q}}_3$, and near-zero when comparing against $\hat{\mathbb{Q}}_4$. The 0th-degree models $\hat{\mathbb{Q}}_3, \hat{\mathbb{Q}}_4$ perform comparable to the 1st-degree model $\hat{\mathbb{P}}$.

Regarding the comparison with $\hat{\mathbb{Q}}_{3,k}$ we may observe in Figure 9(b) that the sign of the KL divergence rate difference is probably positive for $k = 1, 2, 4$, possibly positive for $k = 3, 11, 12$ but not much, possibly negative for $k = 6, 7, 8$ but not much, and inconclusive for $k = 5, 9, 10$. The downward trend for small k suggests that a strictly positive number of free parameters in the cluster transition matrix are necessary to accurately represent the data. Judging from the KL divergence rate difference at $k \approx 7$, in which case the number of degrees of freedom in both models are equal, it appears that the specific freedoms allowed in $\hat{\mathbb{P}}$ give a performance comparable to that attained by the specific freedoms allowed in $\hat{\mathbb{Q}}_{3,7}$.

8.4.3 Comparing the histogram of singular values to the limiting distribution of singular values of the inferred BMC

Figure 9(c) depicts histograms of singular values, and the models $\hat{\mathbb{P}}, \hat{\mathbb{Q}}_1, \hat{\mathbb{Q}}_2, \hat{\mathbb{Q}}_3, \hat{\mathbb{Q}}_4$'s corresponding theoretical predictions. All theoretical predictions were calculated from the training data, while the histograms of singular values were calculated from the validation data.

Observe that all theoretical predictions give a fair description of the laws. Models $\hat{\mathbb{P}}, \hat{\mathbb{Q}}_4$ outperform models $\hat{\mathbb{Q}}_1, \hat{\mathbb{Q}}_2, \hat{\mathbb{Q}}_3$ when it comes to describing the distribution of singular values of $\hat{N}_{\text{validation}}/\sqrt{n}$. Observe that the empirical observations for $\sqrt{n}\hat{L}_{\text{validation}}$ as well as the predictions associated to $\hat{\mathbb{P}}, \hat{\mathbb{Q}}_1, \hat{\mathbb{Q}}_2, \hat{\mathbb{Q}}_3, \hat{\mathbb{Q}}_4$ all appear to be quarter-circular. This quarter-circular law is consistent with our suspicion of a strong 0th-degree model component: in a 0th-degree BMC, the limiting law of $\sqrt{n}\hat{L}$ is known to be quarter-circular. The peek at zero in the empirical observations is likely due to the sparsity.

8.4.4 Conclusion

In all considered performance measures we saw that the 1st-degree BMC model $\hat{\mathbb{P}}$ performed approximately equally well as the 0th-degree models $\hat{\mathbb{Q}}_3, \hat{\mathbb{Q}}_4$. The consideration of the models $\hat{\mathbb{Q}}_{3,k}$ suggested that one further requires a certain number of parameters to achieve sufficient model expressivity.

The sparsity of the data makes it difficult to come to a definitive conclusion since the confidence bounds remain rather

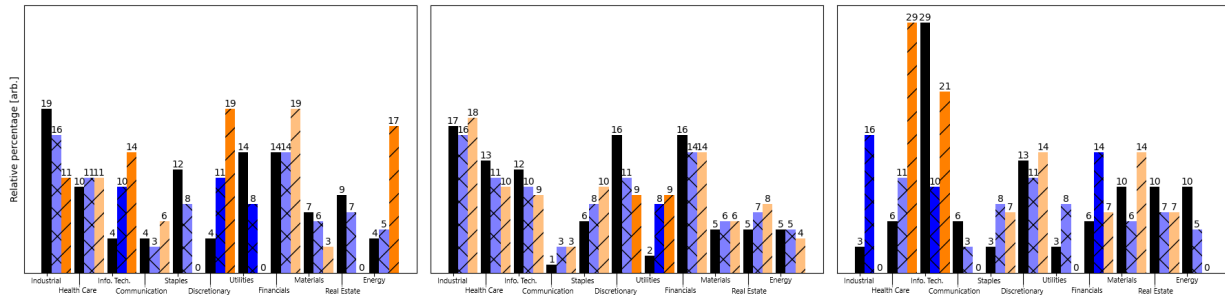


Fig. 8. The relative percentages of constituents in each sector within the 300 constituents under consideration for models $\hat{\mathbb{P}}$, $\hat{\mathbb{Q}}_1$ and $\hat{\mathbb{Q}}_2$ corresponding to the black, blue and orange bars respectively. The left, middle, and right plots correspond to the 1st largest, 2nd largest, and 3rd largest detected cluster, respectively. A bar's color is more saturated when the difference in relative percentage exceeds 5% when compared to the black bars. Observe for instance that for the black bars representing $\hat{\mathbb{P}}$ the absence of consumer discretionary in the 1st cluster is noteworthy, just like the absence of most utilities constituents in the 2nd and 3rd cluster, as well as the absence of industrial and health care constituents in the 3rd cluster.

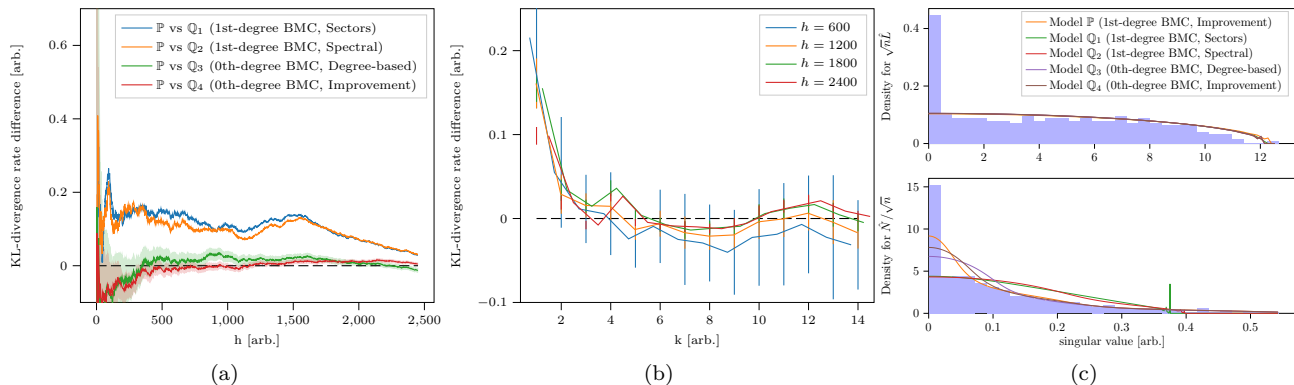


Fig. 9. (a) The KL divergence rate difference estimator $D(X_{\lfloor \ell/2 \rfloor + 1 : \lfloor \ell/2 \rfloor + h}; \hat{\mathbb{P}}^{X_{1: \lfloor \ell/2 \rfloor}}, \hat{\mathbb{Q}}_i^{X_{1: \lfloor \ell/2 \rfloor}})$ on the validation data. The 95% confidence bounds were estimated using (44) in Supplement 13. The mixing time was (somewhat arbitrarily) guessed to be 20 market days. (b) The KL divergence rate difference estimator $\hat{D}(X_{\lfloor \ell/2 \rfloor + 1 : \lfloor \ell/2 \rfloor + h}; \hat{\mathbb{P}}^{X_{1: \lfloor \ell/2 \rfloor}}, \hat{\mathbb{Q}}_{3,k}^{X_{1: \lfloor \ell/2 \rfloor}})$ for different sample path lengths $h \in \mathbb{N}_+$, and as a function of k . The 95% confidence bounds were estimated using (44) in Supplement 13. The mixing time was (somewhat arbitrarily) guessed to be 20 market days. (c) The top and bottom figures display the singular values of the Laplacian $\sqrt{n}\hat{L}$ and the empirical frequency matrix \hat{N}/\sqrt{n} respectively. Both figures were calculated from all $n = 300$ constituents and exclude the $K = 3$ leading singular values.

large. Still, one generally prefers models with fewer parameters. Hence, in our opinion, a 0th-order BMC would be a suitable model for this dataset.

9 Detected orders within the data

In this section, we consider the sequence of clusters $Y_{1:\ell} = \sigma_n(X_{1:\ell})$ provided by the clustering algorithm and select the order of the MC that best fits the data. We look at model selection described in Section 6.3 for the order in the chain using an information criterion. We will focus on the DNA, GPS, and the S&P500 dataset. The Wikipedia dataset is not considered due to its impractical size, and because it does not consist of a single sample path but rather a number of small sample paths. We compute information criteria for all datasets, except for when we study the power of the test. For this task we then focus just on the DNA dataset and the S&P500 dataset.

9.1 Results

We compute (22) for $r = 0, 1, 2, 3, 4$ of the following models:

$\hat{\mathbb{Q}}^{r, \text{MLE}}$: The Maximum-Likelihood Estimator of a r th-order MC estimated from the observation sequence $Y_{1:\ell}$.

The result are in Table 2. We see that the magnitude of the CAIC in Table 2 depends strongly on the observation

r	DNA	incr. (%)	GPS($\times 10^3$)	incr. (%)	S&P500	incr. (%)
0	432650	n.a.	960.63	n.a.	9853	n.a.
1	431502	-0.27	626.54	-34.8	9860	+0.07
2	431263	-0.06	571.49	-40.5	9940	+0.81
3	435228	+0.69	1121.90	+16.8	10253	+3.1
4	458512	+5.3	9789.27	+1019	11162	+8.9

TABLE 2

The CAIC in (22) for the different datasets. Note that the relative difference between the values pertaining to different orders is often small. For example, the differences are less than 0.1% between orders 1, 2 for the DNA data, and between orders 0, 1 for the stock market data. This is not the case, however, with the animal data.

sequence and the number of clusters. In particular, for the GPS dataset the differences are notable for most orders due to the large number of clusters $K = 15$, where higher orders become highly penalized. For the DNA dataset, the criterion suggests that orders $r \in \{1, 2\}$ best approximate the data. For the S&P500 dataset, on the other hand, orders $r \in \{0, 1\}$ appear to be the best. We expect that there is a large variance in Table 2 and some over or underfitting the order is possible. The criterion indicates nonetheless that the transitions of the found clusters, except maybe for the S&P500 dataset, can be

better approximated by a nonzero order Markovian process. We will now support this conclusion empirically with the error models for the DNA and S&P500 datasets.

9.2 Evaluation of the CAIC criterion

In order to probe how significant the information criteria are, we will use the empirical transition law $\hat{\mathbb{P}}^{r,\text{MLE}}$ from the original data $X_{1:\ell}$, which we remark is on the full state space $[n]$. With $\hat{\mathbb{P}}^{r,\text{MLE}}$ for $r \in \{0, 1\}$ we will consider two data-generating models with errors determined by a parameter $\varepsilon \in [0, 1)$, and then look at the clustered process Y_ε^r generated by these models. The models are:

\mathbb{W}_ε^1 : A perturbed 1st-order BMC with probability distribution $\hat{\mathbb{P}}^{1,\text{MLE}}$ and a perturbation given by a heavy-tailed 0th-order perturbation defined in Section 3.2. In contrast to the perturbed models described in Section 3.2, the perturbation here is assumed to be a 0th-order MC.

\mathbb{W}_ε^0 : A perturbed 0th-order BMC with probability distribution $\hat{\mathbb{P}}^{0,\text{MLE}}$ and a perturbation given by a heavy-tailed 1st-order MC defined in Section 3.2.

Assume that we are interested in a particular criterion $C: [K]^{\ell+1} \times [0, 1]^{K \times K} \rightarrow \mathbb{R}$ such as the CAIC. Denote $Y_{1:\ell}^{r,\varepsilon} = \sigma_n(X_{1:\ell}^\varepsilon)$ the cluster process if $X_{1:\ell}^\varepsilon \sim \mathbb{W}_\varepsilon^r$. We will study the robustness of the criterion by examining how often it over- and underfits when selecting s for the models $\hat{\mathbb{Q}}^{s,\text{MLE}}$ with the clustered sequence $Y_{1:\ell}^{r,\varepsilon}$. To study this aspect, we will consider two targets for the CAIC and restrict to the orders $r \in \{0, 1\}$. The first target is the overfit error probability

$$e_{\text{over}}(\varepsilon) := \mathbb{P}_{X_{1:\ell}^\varepsilon \sim \mathbb{W}_\varepsilon^0}(\text{argmin}_{r \in \{0,1\}} \text{CAIC}(Y_{1:\ell}^{r,\varepsilon}) = 1), \quad (31)$$

that is, the probability that the criterion selects a 1st-order process for the chain of cluster transitions when the underlying generating process is $\hat{\mathbb{P}}^{0,\text{MLE}}$ and the only higher order contributions come from perturbations. The second target is the underfit error probability defined as

$$e_{\text{under}}(\varepsilon) := \mathbb{P}_{X_{1:\ell}^\varepsilon \sim \mathbb{W}_\varepsilon^1}(\text{argmin}_{r \in \{0,1\}} \text{CAIC}(Y_{1:\ell}^{r,\varepsilon}) = 0), \quad (32)$$

that is, the probability that the criterion selects a 0th-order process as the best-candidate while $\hat{\mathbb{P}}^{1,\text{MLE}}$ is the actual underlying data-generating process.

We will look at parameters retrieved from the DNA and S&P500 datasets. Because the S&P500 dataset is the least clear dataset, we also consider a synthetic observation sequence. This synthetic observation sequence is generated using the same model \mathbb{W}_ε^r as is obtained for the stock market, but will be five times as long: $5\ell_{\text{SM}}$, where ℓ_{SM} is the length of the path of the S&P500 dataset. We will refer to this synthetic observation sequence as the ‘‘extended stock market model.’’ In this manner we can see the effect of sparsity on the criterion robustness *as if* we could have access to more data.

In Figure 10, the error probabilities as well as centered CAIC values can be seen. We see that both the underfit $e_1(\varepsilon)$ and overfit error $e_2(\varepsilon)$ are usually small for small ε . The overfit error is, however, considerably larger for the DNA dataset than for the S&P500 dataset. This supports the claim that the CAIC chooses the model with fewest parameters for the same amount of information, that is, the criterion is less prone to overfit when the data is sparse. The underfit error is on the contrary small for the DNA dataset, also for $\varepsilon \in [0.1, 0.2]$. This

suggests that order selection via information criteria is robust to misclassification error.

The case of the S&P500 dataset is especially interesting. In Table 2, the criterion chooses $r = 0$ whereas in the \mathbb{W}_ε^1 model in Figure 10(a)–(b), the criterion selects $r = 1$ up to $\varepsilon \sim 0.1$. Afterwards, deviating from the BMC model by just 1 out of 10 jumps in the S&P500 dataset will make the criterion behave similarly as in Table 2. This is also supported by Figure 10(b), where the difference between the criterion for $r = 0$ and $r = 1$ in the S&P500 dataset takes values in $[0, 10]$, which we coincidentally also see in Table 2. This suggests that there may be a 1st-order Markovian structure in the S&P500 dataset but also a strong degree dependence (or 0th-order process). Alternatively, the data may simply be too sparse for the CAIC to select a suitable order. This hypothesis is also supported by the stock market extended dataset, where model selection with five times more data has fewer such problems.

We finally remark that looking at information criteria for the unclustered observation sequences $X_{1:\ell}$ provides no useful insights due to the large dimensionality of the models. In particular, the CAIC criteria for the unclustered observation sequences for order $r \in \{0, 1\}$ can be seen in Table 3. As the data shows, the CAIC criteria just picks the model with smallest number of parameters. This is even more extreme in the GPS and S&P500 datasets, where on top of large model dimension we have sparse data.

r	DNA	GPS	S&P500
0	1339.5×10^3	2943×10^3	54.27×10^3
1	1361.9×10^3	$\approx 1 \times 10^8$	882×10^3

TABLE 3

The CAIC in (22) for the sequence X_1, \dots, X_ℓ for different datasets.

9.3 Conclusion

The main takeaways of this section are as follows:

- Model selection is feasible if we use the clustered sequence $Y_{1:\ell} = \sigma_n(X_{1:\ell})$ obtained after the clustering algorithm. This namely reduces the amount of free parameters of the models considerably.
- For the DNA and GPS datasets, the CAIC selects a nonzero order MCs.
- For the S&P500 dataset the CAIC shows that the data is too sparse for selecting a specific order with certainty. However, there are indications that the values obtained in the CAIC for the S&P500 dataset are consistent with a 1st-order BMC model with a strong 0th-order MC baseline.

10 Conclusions

We have found that using a BMC model for exploratory data analysis in unlabeled observation sequences does in fact produce useful insights. Although there is no guarantee that there are clusters or that a cluster structure is actually revealing of a ground truth model we can still evaluate the clusters and associated models. The DNA example uncovered known, nontrivial and biologically relevant structure. In the text-based example, the improvement algorithm enhanced performance on down-stream tasks and the spectral noise

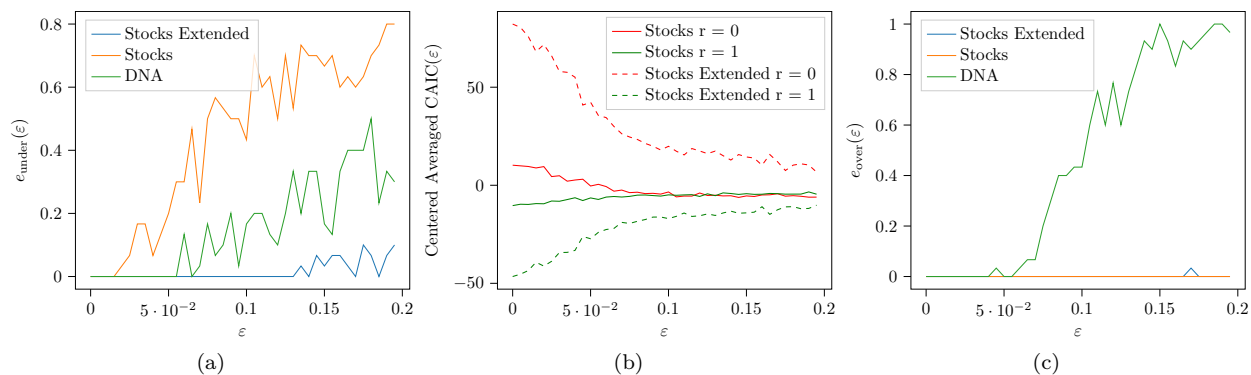


Fig. 10. (a) Underfit error probability $e_{\text{under}}(\varepsilon)$ in (32) depending on the perturbation ε for the DNA, S&P500 dataset, and extended S&P500 datasets assuming the data-generating process is $\mathbb{W}_{\varepsilon}^1$ for their respective datasets. Note the effect of reducing sparsity for the extended S&P500 dataset in reducing the underfit error probability. The plot suggests that the probability of underfitting for small ε , while nonzero, is less than the probability of selecting the correct order. (b) Centered average of CAIC for the S&P500 dataset and S&P500 dataset extended datasets assuming the data-generating process is $\mathbb{W}_{\varepsilon}^1$. Note that the criterion cannot already select the correct order for the S&P500 dataset after $\varepsilon \sim 0.08$. However, by increasing the dataset size 5-fold, it can very robustly select the correct order even for larger error ε . We remark that the empirical variance is an order of magnitude too large to be represented in the plot ($\text{Var}(\text{CAIC}(Y_{1:\ell}(\varepsilon))) \simeq O(10^2)$). Despite this very large variance, the selection process is robust for small error ε . (c) Overfit error probability $e_{\text{over}}(\varepsilon)$ depending on the perturbation ε for the DNA, S&P500 dataset, and extended S&P500 datasets assuming the data-generating process is $\mathbb{W}_{\varepsilon}^0$. Compared to the underfit error probability, the CAIC is robust at selecting a model with lower order, provided there is enough information. In particular, for the DNA, the 1st-order perturbation becomes dominant in the criterion fairly quickly after $\varepsilon > 0.05$. In all tests the number of repetitions was $R = 30$.

identified the heavy-tailed nature of some model violations. The animal movement example uncovered features which could not have been extracted from only the GPS coordinates. For the daily best performing stocks in the S&P500, we saw that a 0th-order BMC can describe its statistical aspects, but there are indications that a 1st-order BMC is also a suitable model.

Acknowledgments

This publication is part of the project *Clustering and Spectral Concentration in Markov Chains* (with project number OCENW.KLEIN.324) of the research programme *Open Competition Domain Science – M* which is (partly) financed by the Dutch Research Council (NWO).

The authors also acknowledge support by the *European Union's Horizon 2020 research and innovation programme* under the Marie Skłodowska-Curie grant agreement no. 945045, and by the *NWO Gravitation project NETWORKS* under grant no. 024.002.003. 

We would finally like to thank Mike van Santvoort for useful discussions while writing this paper.

References

- [1] A. Zhang and M. Wang, "Spectral state compression of Markov processes," *IEEE Transactions on Information Theory*, 2019.
- [2] J. Sanders, A. Proutière, and S.-Y. Yun, "Clustering in Block Markov Chains," *The Annals of Statistics*, 2020.
- [3] S. Singh, T. Jaakkola, and M. Jordan, "Reinforcement Learning with soft state aggregation," *Advances in Neural Information Processing Systems*, 1994.
- [4] R. Ortner, "Adaptive Aggregation for Reinforcement Learning in Average Reward Markov Decision Processes," *Annals of Operations Research*, 2013.
- [5] J. Sanders and A. Van Werde, "Singular value distribution of dense random matrices with block Markovian dependence," *arXiv preprint arXiv:2204.13534*, 2022.
- [6] J. Sanders and A. Senen-Cerda, "Spectral norm bounds for Block Markov Chain random matrices," *arXiv preprint arXiv:2111.06201*, 2021.
- [7] Y. Duan, T. Ke, and M. Wang, "State aggregation learning from Markov transition data," *Advances in Neural Information Processing Systems*, 2019.
- [8] S. Bi, Z. Yin, and Y. Weng, "A low-rank spectral method for learning Markov models," *Optimization Letters*, 2022.
- [9] Z. Du, N. Ozay, and L. Balzano, "Mode clustering for Markov jump systems," in *2019 IEEE 8th International Workshop on Computational Advances in Multi-Sensor Adaptive Processing (CAMSAP)*, 2019.
- [10] Z. Zhu, X. Li, M. Wang, and A. Zhang, "Learning Markov models via low-rank optimization," *Operations Research*, 2021.
- [11] C. Gao, Z. Ma, A. Y. Zhang, and H. H. Zhou, "Achieving optimal misclassification proportion in Stochastic Block Models," *The Journal of Machine Learning Research*, 2017.
- [12] S. Fortunato, "Community detection in graphs," *Physics Reports*, 2010.
- [13] S. Zolhavarieh, S. Aghabozorgi, and Y. W. Teh, "A Review of Subsequence Time Series Clustering," *The Scientific World Journal*, 2014.
- [14] S. Aghabozorgi, A. S. Shirkhorshidi, and T. Y. Wah, "Time-series clustering – A decade review," *Information Systems*, 2015.
- [15] T. W. Liao, "Clustering of time series data – A survey," *Pattern Recognition*, 2005.
- [16] J. Lin, E. Keogh, and W. Truppel, "Clustering of Streaming Time Series is Meaningless," in *Proceedings of the 8th ACM SIGMOD workshop on Research Issues in Data Mining and Knowledge Discovery*, 2003.
- [17] T. Rakthanmanon, E. J. Keogh, S. Lonardi, and S. Evans, "Time series epenthesis: Clustering time series streams requires ignoring some data," in *2011 IEEE 11th International Conference on Data Mining*, 2011.
- [18] S. Rodpongpun, V. Niennattrakul, and C. A. Ratanamahatana, "Selective subsequence time series clustering," *Knowledge-Based Systems*, 2012.
- [19] A. Gionis and H. Mannila, "Finding Recurrent Sources in Sequences," in *Proceedings of the seventh annual international conference on Research in computational Molecular Biology*, 2003.
- [20] A. Ultsch and F. Mörchen, *ESOM-Maps: Tools for clustering, visualization, and classification with Emergent SOM*. 2005.
- [21] F. Mörchen, A. Ultsch, and O. Hoos, "Extracting interpretable muscle activation patterns with time series knowledge mining," *International Journal of Knowledge-based and Intelligent Engineering Systems*, 2005.
- [22] O.-A. Maillard and S. Mannor, "Latent bandits," in *International Conference on Machine Learning*, 2014.
- [23] M. G. Azar, A. Lazaric, and E. Brunskill, "Sequential transfer

- in Multi-Armed Bandit with finite set of models,” *Advances in Neural Information Processing Systems*, 2013.
- [24] L. Li, T. J. Walsh, and M. L. Littman, “Towards a unified theory of state abstraction for MDPs,” in *AI&M*, 2006.
- [25] H. Y. Ong, “Value function approximation via low-rank models,” *arXiv preprint arXiv:1509.00061*, 2015.
- [26] K. Azizzadenesheli, A. Lazaric, and A. Anandkumar, “Reinforcement Learning in rich-observation MDPs using spectral methods,” *arXiv preprint arXiv:1611.03907*, 2016.
- [27] Y. Yang, G. Zhang, Z. Xu, and D. Katabi, “Harnessing structures for value-based planning and Reinforcement Learning,” *arXiv preprint arXiv:1909.12255*, 2019.
- [28] A. A. Markov, “Primer statisticheskogo issledovaniya nad tekstom ‘evgeniya onegina’, illyustriruyuschij svyaz’ispytaniy v cep’,” *Izvestiya Akademii Nauk*, 1913.
- [29] C. Manning and H. Schütze, *Foundations of Statistical Natural Language Processing*. 1999.
- [30] H. Almagor, “A Markov analysis of DNA sequences,” *Journal of Theoretical Biology*, 1983.
- [31] R. Jorre and R. Curnow, “A model for the evolution of the proteins: Cytochrome c: mammals, reptiles, insects,” *Biochimie*, 1976.
- [32] S. Robin, F. Rodolphe, and S. Schbath, *DNA, words and models: statistics of exceptional words*. 2005.
- [33] I. Gialampoukidis, K. Gustafson, and I. Antoniou, “Time operator of Markov chains and mixing times. Applications to financial data,” *Physica A: Statistical Mechanics and its Applications*, 2014.
- [34] D. Zhang and X. Zhang, “Study on forecasting the stock market trend based on stochastic analysis method,” *International Journal of Business and Management*, 2009.
- [35] J. van der Hoek and R. J. Elliott, “Asset pricing using finite state Markov chain stochastic discount functions,” *Stochastic Analysis and Applications*, 2012.
- [36] R. S. Mamon and R. J. Elliott, *Hidden Markov Models in Finance*. 2007.
- [37] P. Billingsley, “Statistical methods in Markov chains,” *The Annals of Mathematical Statistics*, 1961.
- [38] M. Menéndez, D. Morales, L. Pardo, and K. Zografos, “Statistical inference for finite Markov chains based on divergences,” *Statistics & Probability Letters*, 1999.
- [39] L. Pardo, *Statistical inference based on divergence measures*. 2018.
- [40] M. Menéndez, J. Pardo, and L. Pardo, “Csiszar’s-divergences for testing the order in a Markov chain,” *Statistical Papers*, 2001.
- [41] F. Barsotti, A. Philippe, and P. Rochet, “Hypothesis testing for Markovian models with random time observations,” *Journal of Statistical Planning and Inference*, 2016.
- [42] H. Akaike, “A new look at the statistical model identification,” *IEEE Transactions on Automatic Control*, 1974.
- [43] H. Bozdogan, “Model selection and Akaike’s Information Criterion (AIC): The general theory and its analytical extensions,” *Psychometrika*, 1987.
- [44] D. Anderson and K. Burnham, “Model selection and multi-model inference,” *Second. NY: Springer-Verlag*, 2004.
- [45] S. Kullback and R. A. Leibler, “On information and sufficiency,” *The Annals of Mathematical Statistics*, 1951.
- [46] J. Ding, V. Tarokh, and Y. Yang, “Model selection techniques: An overview,” *IEEE Signal Processing Magazine*, 2018.
- [47] National Library of Medicine, “OCA2 melanosomal transmembrane protein homo sapiens (human).” <https://www.ncbi.nlm.nih.gov/gene/4948>, 2021. Accessed in October 2021, RefSeq Accession NC_000015.10.
- [48] B. Wilson, “The Unknown Perils of Mining Wikipedia.” <https://www.lateral.io/resources-blog/the-unknown-perils-of-mining-wikipedia>, June 2015.
- [49] S. Bird, E. Klein, and E. Loper, *Natural language processing with Python: analyzing text with the natural language toolkit*. 2009.
- [50] D. L. Stephen Blake, Randy Arndt, “Movebank.” https://www.movebank.org/cms/webapp?gwt_fragment=page=studies,path=study8019591, 2017. Accessed: 2022-08-16.
- [51] Alpha Vantage Co, “Stock data API,” 2021.
- [52] G. A. Gutman and G. W. Hatfield, “Nonrandom utilization of codon pairs in *Escherichia coli*,” *Proceedings of the National Academy of Sciences*, 1989.
- [53] J. R. Coleman, D. Papamichail, S. Skiena, B. Futcher, E. Wimmer, and S. Mueller, “Virus Attenuation by Genome-Scale Changes in Codon Pair Bias,” *Science*, 2008.
- [54] D. Kunec and N. Osterrieder, “Codon Pair Bias Is a Direct Consequence of Dinucleotide Bias,” *Cell Reports*, 2016.
- [55] B. Irwin, J. D. Heck, and G. W. Hatfield, “Codon Pair Utilization Biases Influence Translational Elongation Step Times,” *Journal of Biological Chemistry*, 1995.
- [56] G. Moura, M. Pinheiro, R. Silva, I. Miranda, V. Afreixo, G. Dias, A. Freitas, J. L. Oliveira, and M. A. Santos, “Comparative context analysis of codon pairs on an ORFeome scale,” *Genome Biology*, 2005.
- [57] A. Alexaki, J. Kames, D. D. Holcomb, *et al.*, “Codon and codon-pair usage tables (CoCoPUTs): facilitating genetic variation analyses and recombinant gene design,” *Journal of Molecular Biology*, 2019.

Supplementary material of “Detection and Evaluation of Clusters within Sequential Data”

11 Pseudo-code describing the clustering procedure

Algorithm 1: Spectral clustering algorithm.

Input: n, K and \hat{N} .
Output: Cluster assignment $\hat{\mathcal{V}}_1, \dots, \hat{\mathcal{V}}_K$

- 1 $\hat{N}_\Gamma \leftarrow \text{Trim}(\hat{N})$;
- 2 $\hat{R} \leftarrow K$ -rank approximation of \hat{N}_Γ ;
- 3 $\hat{\mathcal{V}}_1, \dots, \hat{\mathcal{V}}_K \leftarrow K$ -means($[\hat{R}, \hat{R}^T]$);

The spectral clustering in Algorithm 1 is used to obtain a good initial estimate for the clusters. A k-means algorithm is used along a K -rank approximation of \hat{N} (or \hat{N}_Γ for the trimmed version of \hat{N}) to yield an initial guess for the clusters. It can be proved, however, that this step yields a number of misclassified states that is sublinear in n but not of constant order [69]. A second step is then required to attain exact recovery. In Algorithm 2, we see that a procedure similar to a likelihood ratio maximization is used to improve the cluster assignment. With this extra step it can be proven that the misclassified states will be order constant in expectation.

Algorithm 2: Cluster improvement algorithm (for 1st-order BMCs)

Input: n, K, ℓ, \hat{N} and initial cluster assignment guess $\hat{\mathcal{V}}_1, \dots, \hat{\mathcal{V}}_K$.
Output: New cluster assignment $\hat{\mathcal{V}}'_1, \dots, \hat{\mathcal{V}}'_K$

- 1 **for** $a \leftarrow 1$ **to** K **do**
- 2 $\hat{\pi}_a \leftarrow \hat{N}_{\hat{\mathcal{V}}_a, [n]} / \ell, \hat{\alpha}_a \leftarrow \#\hat{\mathcal{V}}_a / n$;
- 3 $\hat{\mathcal{V}}'_a \leftarrow \emptyset$;
- 4 **for** $b \leftarrow 1$ **to** K **do**
- 5 $\hat{p}_{a,b} \leftarrow \hat{N}_{\hat{\mathcal{V}}_a, \hat{\mathcal{V}}_b} / \hat{N}_{\hat{\mathcal{V}}_a, [n]}$;
- 6 **end**
- 7 **end**
- 8 **for** $x \leftarrow 1$ **to** n **do**
- 9 $c \leftarrow \text{argmax}_{l \in [K]} \sum_{k=1}^K (\hat{N}_{x, \hat{\mathcal{V}}_k} \ln(\hat{p}_{l,k}) + \hat{N}_{\hat{\mathcal{V}}_k, x} \ln(\hat{p}_{k,l} / \hat{\alpha}_l)) - \frac{\ell}{n} \frac{\hat{\pi}_l}{\hat{\alpha}_l}$;
- 10 $\hat{\mathcal{V}}'_c \leftarrow \hat{\mathcal{V}}'_c \cup \{x\}$;
- 11 **end**

12 Robustness of the clustering procedure to model violations

Recall that the asymptotic consistency of the clustering procedure has been theoretically studied in [69] under the assumption that the data-generating process is a BMC. In this section we aim to study the robustness of the clustering procedure to violations of this model assumption. That is, we investigate the performance of the clustering procedure when the data-generating process is not actually a BMC. We study two main measures of performance. First, in Supplement 12.1, we consider the number of misclassified states. Second, in Supplement 12.2, we consider the approximation error in a parameter estimation problem where the objective is to estimate the true transition matrix P of a Markovian data-generating process which need-not be a BMC.

The first measure of performance requires that the notion of misclassification is sensible even though the data-generating process is not a BMC. To this end we restrict ourselves to models where communities are still well-defined. More precisely, we consider the perturbed BMC model which was defined in Section 3.2 and assign as ground-truth communities those of the BMC-kernel which was used to construct the perturbed model. Recall that the definition of a perturbed BMC requires to specify the nature of the perturbation kernel Δ . The following kernels are used for this purpose to model different types of model violations:

- (i) *Uniform Stochastic:* The matrix Δ is sampled uniformly at random in the set of stochastic matrices. This is accomplished by sampling each row independently from a Dirichlet($1/n, \dots, 1/n$) distribution.
- (ii) *Degree 0:* Fix some $\pi_1, \dots, \pi_n > 0$ with $\sum_{i=1}^n \pi_i = 1$ and let $\Delta_{ij} = \pi_j$ for all $i, j \in [n]$. We construct the π_i by sampling independent exponential random variables $e_1, \dots, e_n \sim \text{Exponential}(1)$ and normalizing $\pi_i = e_i / (\sum_{j=1}^n e_j)$.
- (iii) *Heavy Tailed:* Let X be a random matrix whose entries X_{ij} are i.i.d. positive random variables with a heavy-tailed distribution. The kernel Δ is then found by normalizing the rows in order to achieve a stochastic matrix $\Delta := \text{diag}((\sum_j X_{ij})^{-1})_{i=1}^n X$. We sample the heavy-tailed entries X_{ij} from a Zipf distribution with exponent $s = 3/2$.
- (iv) *Sparse:* Consider constants $d > 0$ and $c > 0$ and construct a random matrix $X = A + cJ$ where A is the adjacency matrix from a directed Erdős-Rényi random graph with average outgoing degree d and J is a constant matrix $J_{ij} = 1/n$. The

kernel Δ is then found by rescaling the rows in order to achieve a stochastic matrix $\Delta = \text{diag}((\sum_j X_{ij})^{-1})_{i=1}^n X$. We take $d = 5$ and $c = 0.1$.

In our subsequent experimentation we take $n = 2m$ to be an even integer. The BMC which is perturbed is chosen to have two equally-sized clusters ($K = 2$) and cluster transition matrix given by

$$p = \begin{pmatrix} 0.6 & 0.4 \\ 0.4 & 0.6 \end{pmatrix}.$$

12.1 Misclassification ratio for perturbed BMCs

This section concerns the number of misclassified states when clustering on a perturbed BMC model. Recall that we chose the BMC model to have two equally-sized clusters which means that we may pick the cluster assignment map to be given by $\sigma_n(i) = 1 + \mathbb{1}[i > n/2]$. Let $\hat{\sigma}_n : [n] \rightarrow \{1, 2\}$ be an estimated cluster assignment which is output by the clustering procedure. Then, the misclassification ratio \mathcal{E} is defined as

$$\mathcal{E} := \frac{1}{n} \min_{\rho \in S_2} \#\{v \in [n] : \sigma_n(v) \neq (\rho \circ \hat{\sigma}_n)(v)\}. \quad (33)$$

Here S_2 denotes the set of permutations of $\{1, 2\}$.

Recall from (9) that the parameter ε of the perturbed BMC measures the fraction of transitions which are affected by the perturbation. In other words, ε measures the strength of the perturbation. The estimated expected misclassification ratio $\mathbb{E}[\mathcal{E}]$ is displayed as a function of the perturbation level ε for a numerical experiment in Figure 2(a). Up to $\varepsilon \approx 0.1$ the algorithm succeeds in recovering the exact cluster assignment for all four models. The exact number will naturally depend on the parameters of the BMC which was perturbed and will consequently be different in different contexts. At any rate, we conclude from this experiment that the algorithm appears to be robust with regards to small to medium-sized model violations.

The observation that some model violations can be tolerated may be understood theoretically in terms of the construction of the algorithm. This robustness is namely natural at the level of the spectral step of the algorithm. Consider that in a perturbed BMC one has the following decomposition:

$$\begin{aligned} \hat{N}_{\text{Perturbed}} &= \mathbb{E}[\hat{N}_{\text{BMC}}] + (\mathbb{E}[\hat{N}_{\text{Perturbed}}] - \mathbb{E}[\hat{N}_{\text{BMC}}]) + (\hat{N}_{\text{Perturbed}} - \mathbb{E}[\hat{N}_{\text{Perturbed}}]) \\ &=: \mathbb{E}[\hat{N}_{\text{BMC}}] + E_{\text{Perturbation}} + E_{\text{Noise}}. \end{aligned}$$

The sampling noise E_{Noise} is small in operator norm relative to $\mathbb{E}[\hat{N}_{\text{BMC}}]$ when the sample path is sufficiently long. It may further be expected that $E_{\text{Perturbation}}$ is small in operator norm whenever the perturbation level ε is small. Now recall that spectral step in the algorithm relies on singular value decomposition to compute a rank- K approximation. The purpose of this rank- K approximation, when the process is truly a BMC, is to separate the sampling noise E_{Noise} from the low-rank signal $\mathbb{E}[\hat{N}_{\text{BMC}}]$. In a small perturbation of a BMC the singular value decomposition will however also regard $E_{\text{Perturbation}}$ as an error term. Consequently, for small perturbations, the spectral step has the beneficial effect that it separates the perturbative error $E_{\text{Perturbation}}$ from the low-rank signal $\mathbb{E}[\hat{N}_{\text{BMC}}]$.

12.2 Bias–variance tradeoff for parameter estimation in a perturbed BMC

It may occur in some cases that one is not interested in the clusterings themselves but rather views them as a means to an end. Consider the scenario where one desires to estimate the transition kernel of a Markovian process which need not be a BMC. Assume that one has prior reason to suspect that there could be some underlying clusters in the data but also that there could be parts of the dynamics which do not respect the clusters. In such a case a perturbed BMC would be a suitable model for the data. Let us emphasize that one is here not intrinsically interested in the BMC-component P_{BMC} but rather desires to estimate the ground-truth $P_{\text{True}} := (1 - \varepsilon)P_{\text{BMC}} + \varepsilon\Delta$. It could however be the case that one can exploit the underlying clusters to improve the performance of estimation.

Assume that one knows the number of underlying clusters K and has access to a sample path $X_0^\varepsilon, \dots, X_\ell^\varepsilon$ of length ℓ of a perturbed BMC. Let \hat{N} also denote the associated empirical frequency matrix. A natural general-purpose estimator for the transition matrix, which does not rely on the existence of clusters, is given by the empirical transition matrix $\hat{P}(\ell)$. The entries of the empirical transition matrix are given by

$$\hat{P}_{\text{Empirical}}(\ell)_{ij} := \begin{cases} \frac{\hat{N}_{ij}}{\sum_{k=1}^n \hat{N}_{ik}}, & \text{if } \hat{N}_{ij} \neq 0 \\ 0, & \text{if } \hat{N}_{ij} = 0. \end{cases} \quad (34)$$

Another estimator may be found by first computing a clustering $\hat{\mathcal{V}}_1, \dots, \hat{\mathcal{V}}_K$. One can then hope that, since $P_{\text{True}} \approx P_{\text{BMC}}$ for $\varepsilon \approx 0$, it would be sufficient to consider an estimator \hat{P}_{BMC} for P_{BMC} whose entries are given by

$$\hat{P}_{\text{BMC}}(\ell)_{ij} := \begin{cases} \frac{1}{\#\hat{\mathcal{V}}_{\sigma_n(j)}} \frac{\sum_{x \in \hat{\mathcal{V}}_{\sigma_n(i)}, y \in \hat{\mathcal{V}}_{\sigma_n(j)}} \hat{N}_{x,y}}{\sum_{m=1}^K \sum_{x \in \hat{\mathcal{V}}_{\sigma_n(i)}, y \in \hat{\mathcal{V}}_m} \hat{N}_{x,y}}, & \text{if } \sum_{x \in \hat{\mathcal{V}}_{\sigma_n(i)}, y \in \hat{\mathcal{V}}_{\sigma_n(j)}} \hat{N}_{x,y} \neq 0 \\ 0, & \text{if } \sum_{x \in \hat{\mathcal{V}}_{\sigma_n(i)}, y \in \hat{\mathcal{V}}_{\sigma_n(j)}} \hat{N}_{x,y} = 0. \end{cases} \quad (35)$$

Finally, for comparison we also consider the following trivial estimator which does not even use the data

$$\hat{P}_{\text{Uniform}}(\ell)_{ij} = \frac{1}{n}.$$

We measure the performance of these estimators as a function of the length of the sample path using the expected estimation error:

$$R_*(\ell) := \mathbb{E}[\|P_{\text{True}} - \hat{P}_*(\ell)\|] \quad \text{where } * \in \{\text{Empirical, BMC, Uniform}\}. \quad (36)$$

Here, $\|\cdot\|$ denotes the operator norm $\|M\| = \sup_{\|v\|_2=1} \|Mv\|_2$.

We conduct a numerical experiment with a state space of size $n = 1000$ and a heavy-tailed perturbation model of perturbation strength $\varepsilon = 0.05$. Figure 2(b) displays estimated values of the expected estimation error $R_*(\cdot)$ as a function of the length ℓ of the sample path. A number of different regimes may be identified. First, the regime where the sample path is very short meaning that $\ell \approx 10^4$. Here the empirical estimator $\hat{P}_{\text{Empirical}}$ and the BMC estimator \hat{P}_{BMC} are both unable to outperform the trivial estimator \hat{P}_{Uniform} . The empirical estimator even performs significantly worse than the trivial estimator in this regime. Second, the regime where sample path is medium-sized meaning that $\ell \approx 10^5$. Here the clustering procedure succeeds and \hat{P}_{BMC} becomes the best-performing estimator. Finally, the regime where the sample path grows long meaning that $\ell > 10^6$. Here the empirical estimator becomes the best-performing estimator. These different regimes can be understood in terms of a bias–variance tradeoff. Namely, consider that for short to medium-sized sample paths the BMC estimator \hat{P}_{BMC} has significantly less variance than the empirical estimator $\hat{P}_{\text{Empirical}}$ due to depending on fewer parameters. This decreased variance is the dominant consideration for the approximation error in this regime. On the other hand, for long sample paths both estimators \hat{P}_{BMC} and \hat{P} have low variance and the bias incurred by the approximation $P_{\text{True}} \approx P_{\text{BMC}}$ becomes dominant.

13 Confidence bounds when estimating $D(\mathbb{T}; \mathbb{P}, \mathbb{Q})$

We here state a concentration inequality from which we deduce the confidence interval in (45). Recall that these confidence intervals are used in Figure 9. The proof is based on a result from [67] whose assumptions we first verify.

Assume that the true process $\{X_t\}_{t \geq 0}$ generating the sequential data X_1, \dots, X_ℓ is a MC, which need not be time-homogeneous. Let us refer to $\{X_t\}_{t \geq 0}$'s law as \mathbb{T} . The mixing time of $\{X_t\}_{t \geq 0}$ is defined as

$$\tau_{\text{mix}} := \min\left\{t \geq 1 : \bar{d}(t) \leq \frac{1}{2}\right\}, \quad (37)$$

where

$$\bar{d}(t) := \max_{1 \leq i \leq \ell-t} \sup_{x, y \in [n]} d_{\text{TV}}(\mathbb{T}[X_{i+t} = \cdot \mid X_i = x], \mathbb{T}[X_{i+t} = \cdot \mid X_i = y]). \quad (38)$$

Here, d_{TV} denotes the *total variation distance*:

$$d_{\text{TV}}(\mathbb{T}[X_{i+t} = \cdot \mid X_i = x], \mathbb{T}[X_{i+t} = \cdot \mid X_i = y]) := \frac{1}{2} \sum_{z \in [n]} |\mathbb{T}[X_{i+t} = z \mid X_i = x] - \mathbb{T}[X_{i+t} = z \mid X_i = y]|. \quad (39)$$

We claim that the MC of transitions $\{E_{X,t}\}_{t \geq 0}$, where $E_{X,t} := (X_t, X_{t+1})$, then has mixing time at most $\tau_{\text{mix}} + 1$. Indeed, observe that for any $t \geq \tau_{\text{mix}} + 1$, $x_1, x_2, y_1, y_2 \in [n]$ and $1 \leq i \leq \ell - t - 1$,

$$\begin{aligned} & \frac{1}{2} \sum_{z_1, z_2 \in [n]} |\mathbb{P}[E_{X,i+t} = (z_1, z_2) \mid E_{X,i} = (x_1, x_2)] - \mathbb{P}[E_{X,i+t} = (z_1, z_2) \mid E_{X,i} = (y_1, y_2)]| \\ &= \frac{1}{2} \sum_{z_1, z_2 \in [n]} \mathbb{P}[X_{i+t+1} = z_2 \mid X_{i+t} = z_1] |\mathbb{P}[X_{i+t} = z_1 \mid X_{i+1} = x_2] - \mathbb{P}[X_{i+t} = z_1 \mid X_{i+1} = y_2]| \end{aligned} \quad (40)$$

$$= \frac{1}{2} \sum_{z_1 \in [n]} |\mathbb{P}[X_{i+t} = z_1 \mid X_{i+1} = x_2] - \mathbb{P}[X_{i+t} = z_1 \mid X_{i+1} = y_2]| \leq \frac{1}{2}. \quad (41)$$

Here, the Markov property was used to conclude (40). The fact that $\mathbb{P}(X_{i+t+1} = \cdot \mid X_{i+t} = z_1)$ defines a probability distribution, together with the assumption that $t \geq \tau_{\text{mix}} + 1$ and the property that $\bar{d}(t)$ is nonincreasing in t , was used to arrive at (41).

Now suppose that we are given two MCs with fixed transition matrices P and Q , whose laws we will refer to as \mathbb{P} and \mathbb{Q} , respectively. Assume furthermore that $\max_{i,j \in [n]} |\ln(P_{i,j}/Q_{i,j})| \leq \delta$ for some $\delta > 0$. For any two sample paths X_1, \dots, X_ℓ and Y_1, \dots, Y_ℓ , it then holds that

$$|\hat{D}(X_1, \dots, X_\ell; P, Q) - \hat{D}(Y_1, \dots, Y_\ell; P, Q)| \leq \frac{2\delta}{\ell} \sum_{t=1}^{\ell-1} \mathbf{1}[E_{X,t} \neq E_{Y,t}]. \quad (42)$$

Consequently, [67, Corollary 2.10] applied to the MC $\{E_{X,t}\}_{t \geq 0}$ yields the desired concentration inequality:

$$\mathbb{P}(|\hat{D}(X_0, \dots, X_\ell; \mathbb{P}, \mathbb{Q}) - D(\mathbb{T}; \mathbb{P}, \mathbb{Q})| > t) \leq 2 \exp\left(\frac{-t^2 \ell^2}{18\delta^2(\tau_{\text{mix}} + 1)}\right). \quad (43)$$

In conclusion: if we are given two MCs with fixed transition matrices P and Q for which $\max_{i,j \in [n]} |\ln P_{i,j}/Q_{i,j}| > 0$, together with an estimate for τ_{mix} , we can then construct for $z \in [0, 1]$ a $100(1-z)\%$ confidence intervals of size

$$c_z := \frac{1}{\ell} \max_{i,j \in [n]} \left| \ln \frac{P_{i,j}}{Q_{i,j}} \right| \sqrt{18(\tau_{\text{mix}} + 1) \ln \frac{2}{z}}. \quad (44)$$

This is to say that

$$\mathbb{P}\left[D(\mathbb{T}; \mathbb{P}, \mathbb{Q}) \in [\hat{D}(X_0, \dots, X_\ell; \mathbb{P}, \mathbb{Q}) - c_z, \hat{D}(X_0, \dots, X_\ell; \mathbb{P}, \mathbb{Q}) + c_z]\right] \geq 1 - z. \quad (45)$$

14 Shape of the spectral noise

Recall that it was stated in Section 6.4 that the spectral noise in \hat{N} can be dominated by an inhomogeneous equilibrium distribution. It was further claimed that the Laplacian \hat{L} does not suffer from this issue. The main goal in this section is to argue that this claim is true.

Some preliminary notation and concepts are introduced in Supplement 14.1 after which a theoretical result concerning the limiting singular value distribution of \hat{L} is established in Supplement 14.2. A model with an inhomogeneous equilibrium distribution is introduced in Supplement 14.3. The claim that \hat{L} can also detect violations to the model assumptions in the presence of an inhomogeneous equilibrium distribution is verified in Supplement 14.4 by a simulation experiment.

14.1 Preliminaries

The *empirical singular value distribution* ν_M of a matrix $M \in \mathbb{R}^{n \times n}$ with singular values $s_1(M) \geq \dots \geq s_n(M)$ is the probability measure on $\mathbb{R}_{\geq 0}$ defined by

$$\nu_M(A) := \frac{1}{n} \#\{i \in [n] : s_i(M) \in A\} \quad (46)$$

for every measurable set $A \subseteq \mathbb{R}$. A sequence of random probability measures $\{\mu_n\}_{n \geq 1}$ on the real line is said to *converge weakly in probability* to a probability measure μ if for every continuous bounded function $f : \mathbb{R} \rightarrow \mathbb{R}$ it holds that $\int f d\mu_n$ converges weakly in probability to $\int f d\mu$. The *symmetrization* of a probability measure μ on the positive real line $\mathbb{R}_{\geq 0}$ is the probability measure μ_{sym} on \mathbb{R} given by

$$\mu_{\text{sym}}(A) := \frac{1}{2}(\mu(\{a : a \in A, a \geq 0\}) + \mu(\{-a : a \in A, a \leq 0\})) \quad (47)$$

for any measurable $A \subseteq \mathbb{R}$. Note that μ can be recovered from its symmetrization since for any measurable $A \subseteq \mathbb{R}_{\geq 0}$ it holds that

$$\mu(A) = 2\mu_{\text{sym}}(A \setminus \{0\}) + \mu_{\text{sym}}(\{0\}). \quad (48)$$

The *Stieltjes transform* of a probability measure μ is the analytic function $s : \mathbb{C}^+ \rightarrow \mathbb{C}^-$ given by $s(z) = \int 1/(z-x)d\mu(x)$. Here, $\mathbb{C}^+ := \{z \in \mathbb{C} : \text{Im}(z) > 0\}$ denotes the upper half-plane and $\mathbb{C}^- := \{z \in \mathbb{C} : \text{Im}(z) < 0\}$ denotes the lower half-plane. The Stieltjes inversion formula [59, Theorem B.8] allows one to recover μ from its Stieltjes transform: for any continuity points $a < b$ of μ ,

$$\mu([a, b]) = -\frac{1}{\pi} \lim_{\varepsilon \rightarrow 0^+} \int_a^b \text{Im}(s(x + \sqrt{-1}\varepsilon)) dx. \quad (49)$$

14.2 Limiting law of singular value distribution of the Laplacian \hat{L}

Fix some positive integer $K \geq 1$ and a transition matrix $p \in \mathbb{R}^{K \times K}$ of an ergodic MC on $[K]$. Denote $\pi \in [0, 1]^K$ for the equilibrium distribution of the MC associated to p . For every $n \geq 1$ consider a partition $\mathcal{V}_1 \cup \dots \cup \mathcal{V}_K = [n]$ of the state space into K nonempty groups \mathcal{V}_i . The subsequent results are concerned with the asymptotic regime where $n \rightarrow \infty$. We here assume that there are $\alpha_1, \dots, \alpha_K > 0$ such that $\#\mathcal{V}_i = \alpha_i n + o(n)$ and $\sum_{i=1}^K \alpha_i = 1$.

Proposition 2. *Let \hat{L} be the empirical normalized Laplacian associated to a sample path X_1, \dots, X_ℓ of the above BMC. Assume that as n tends to infinity it holds that $\ell = \lambda n^2 + o(n^2)$. Then, the empirical singular value distribution $\nu_{\sqrt{n}\hat{L}}$ converges weakly in probability to a compactly supported probability measure ν on $\mathbb{R}_{\geq 0}$. Moreover, the symmetrization ν_{sym} has Stieltjes transform $s(z) = \sum_{i=1}^K \alpha_i (a_i(z) + a_{K+i}(z))/2$ where a_1, \dots, a_{2K} are the unique analytic function from \mathbb{C}^+ to \mathbb{C}^- such that the following system of equations is satisfied*

$$a_i(z)^{-1} = z - \sum_{j=1}^K \lambda^{-1} \pi(j)^{-1} \alpha_j p_{ij} a_{K+j}(z), \quad (50)$$

$$a_{i+K}(z)^{-1} = z - \sum_{j=1}^K \lambda^{-1} \pi(i)^{-1} \alpha_j p_{j,i} a_j(z) \quad (51)$$

for $i = 1, \dots, K$.

The proof of Proposition 2 is similar to the proof of [70, Theorem 1.2] which is there given below [70, Proposition 4.7]. The intermediate [70, Lemma 4.4(ii)] should however be replaced by Lemma 1 below, and the role of [70, Equation (22)] is taken over by Lemma 2 below.

Lemma 1. *Let $\Pi_X \in [0, 1]^n$ denote the equilibrium distribution of the BMC, and define*

$$\hat{Q} := \text{diag}((\ell + 1)\Pi_X)^{-1/2}(\hat{N} - \mathbb{E}[\hat{N}])\text{diag}((\ell + 1)\Pi_X)^{-1/2}. \quad (52)$$

Assume that $\nu_{\sqrt{n}\hat{Q}}$ converges weakly in probability to some probability measure ν on $\mathbb{R}_{\geq 0}$. Under the assumptions of Proposition 2, it then holds that $\nu_{\sqrt{n}\hat{L}}$ converges weakly in probability to ν .

Proof. Consider the following notation:

$$\begin{aligned} C_n &:= \text{diag}((\ell + 1)\Pi_X)^{-1/2}\mathbb{E}[\hat{N}]\text{diag}((\ell + 1)\Pi_X)^{-1/2}, \\ D_{n,l} &:= \text{diag}\left(\left(\sum_{k=1}^n \hat{N}_{ik}\right)_{i=1}^n\right)^{-1/2} \text{diag}((\ell + 1)\Pi_X)^{1/2}, \\ D_{n,r} &:= \text{diag}((\ell + 1)\Pi_X)^{1/2} \text{diag}\left(\left(\sum_{k=1}^n \hat{N}_{kj}\right)_{j=1}^n\right)^{-1/2}. \end{aligned} \quad (53)$$

Observe that $\hat{L} = D_{n,l}\hat{Q}D_{n,r} + C_n$. Furthermore, $\max_{i=1}^n |(\ell + 1)^{-1}\Pi_{X,i}^{-1} \sum_{k=1}^n \hat{N}_{ik} - 1|$ converges to zero in probability by [70, Corollary 6.11]. Since $x \mapsto 1/\sqrt{x}$ is continuous in the neighborhood of 1 and the operator norm of a diagonal matrix is the maximal value on its diagonal, it follows that $\|D_{n,l} - \text{Id}\|_{\text{op}}$ converges to zero in probability.

Note that transitions coming into state i are almost in bijection with the outgoing transitions out of state i . The only possible exceptions occur when $i = X_1$ or $i = X_\ell$. This is to say that for every i

$$\left| \sum_{k=1}^n \hat{N}_{ik} - \sum_{k=1}^n \hat{N}_{kj} \right| \leq 2. \quad (54)$$

Hence, using that $(\ell + 1)\Pi_{X,i} = \Theta(n)$ and the fact that we already know that $\max_{i=1}^n |(\ell + 1)^{-1}\Pi_{X,i}^{-1} \sum_{k=1}^n \hat{N}_{ik} - 1|$ converges to zero in probability, it follows that $\max_{i=1}^n |(\ell + 1)^{-1}\Pi_{X,i}^{-1} \sum_{k=1}^n \hat{N}_{ki} - 1|$ converges to zero in probability. By the continuity of $1/\sqrt{x}$ near 1 we may now also conclude that $\|D_{n,r} - \text{Id}\|_{\text{op}}$ converges to zero in probability.

By two applications of [70, Lemma 6.8.(iii)] we conclude that $\nu_{\sqrt{n}D_{n,l}\hat{Q}D_{n,r}}$ converges weakly in probability to ν .

Further, by the fact that the BMC starts in equilibrium it holds that $\text{rank}(\mathbb{E}[\hat{N}]) \leq K$. Hence, using the general fact that $\text{rank}(AB) \leq \text{rank}(A)$ for any two matrices A, B of compatible size, we find that

$$\text{rank}(\sqrt{n}C_n) \leq \text{rank}(\mathbb{E}[\hat{N}]) \leq K. \quad (55)$$

An application of [70, Lemma 6.8.(ii)] now yields the desired result, since $\nu_{\sqrt{n}\hat{L}} = \nu_{\sqrt{n}(D_{n,l}\hat{Q}D_{n,r} + C_n)}$. \square

Lemma 2. *Under the assumptions of Proposition 2 and with notation as in Lemma 1 it holds that as n tends to infinity*

$$\max_{ij=1, \dots, n} |\text{Var}[\hat{Q}_{ij}] - \lambda^{-1}\pi(\sigma_n(j))^{-1}p_{\sigma_n(i)\sigma_n(j)}| = o(1). \quad (56)$$

Proof. This is immediate from [70, Corollary 4.6] using the fact that $\text{Var}[cX] = c^2 \text{Var}[X]$ for any real random variable X and scalar $c \in \mathbb{R}$. \square

14.3 Inhomogeneous equilibrium distribution: Degree-corrected block Markov chain (DC-BMC)

In order to allow for an inhomogeneous equilibrium distribution we consider the following model which is inspired by the analogous degree-corrected stochastic block model for communities in graphs with inhomogeneous degrees. Let $K \geq 1$ be a positive integer, consider a transition matrix $p \in \mathbb{R}^{K \times K}$ for an ergodic MC on $[K]$ and equip the state-space with a group-assignment map $\sigma_n : [n] \rightarrow [K]$. As was the case for BMCs we define the groups $\mathcal{V}_1, \dots, \mathcal{V}_K$ by $\mathcal{V}_i = \{v \in [n] : \sigma_n(v) = i\}$. Assume moreover that every group \mathcal{V}_i is equipped with a probability distribution $\mu_i : \mathcal{V}_i \rightarrow [0, 1]$. Then, a MC X_t on $[n]$ is called a DC-BMC if

$$\mathbb{P}(X_{t+1} = j \mid X_t = i) = p_{\sigma_n(i)\sigma_n(j)}\mu_{\sigma_n(j)}(j). \quad (57)$$

Recall that in a BMC it holds that conditional on $\sigma_n(X_t) = k$ for $t > 1$ the observation X_t is chosen uniformly at random in the cluster \mathcal{V}_k . In a DC-BMC it instead holds that conditional on $\sigma_n(X_t) = k$ the observation X_t is chosen from the cluster \mathcal{V}_k according to the probability measure μ_k .

Note that the usual BMC is recovered when all μ_i are taken to be the uniform measures on their respective groups \mathcal{V}_i . Furthermore, by taking a larger number of groups $\tilde{K} = MK$ one can still approximate a DC-BMC model by a BMC-model. This is to say that one can use the additional clusters to separate each true group \mathcal{V}_i of the DC-BMC model into M subgroups $\tilde{\mathcal{V}}_{i,1}, \dots, \tilde{\mathcal{V}}_{i,M}$ such that μ_i is approximately constant on every $\tilde{\mathcal{V}}_{i,j}$.

We expect that the limiting measure for $\nu_{\sqrt{n}\hat{L}}$ in a DC-BMC is equal to the limiting measure of a BMC with the same cluster transition matrix p and the same cluster ratios α_i provided that $\max_{i=1,\dots,n} \mu_{\sigma_n(i)}(i) = \Theta(1/n)$ and $\min_{i=1,\dots,n} \mu_{\sigma_n(i)}(i) = \Theta(1/n)$. If this conjecture is true then the limiting measure does not depend at all on the μ_i since these do not occur in Proposition 2. The insensitivity to the μ_i allows to ensure that the spectral noise in \hat{L} is not dominated by an inhomogeneous equilibrium distribution. The main reason for this conjecture is that the proof of Proposition 2 implicitly relies on a universality principle of [70] which states that the limiting singular value distribution in a (sufficiently well-behaved) random matrix only depends on the variance of its entries. We will namely subsequently argue that the variance profile of \hat{L} is approximately independent of distributions μ_k ; see (64).

Denote π for the cluster equilibrium distribution of the Markov chain associated to p and note that the state equilibrium distribution of a DC-BMC is then given by $\Pi_{X,i} = \pi(\sigma_n(i))\mu_{\sigma_n(i)}$. Correspondingly, up to approximation errors on the order of $\sqrt{\ell}$,

$$\sum_{k=1}^n \hat{N}_{i,k} \approx \#\{t = 1, \dots, \ell : X_t = i\} \approx \ell \Pi_{X,i} = \ell \pi(\sigma_n(i))\mu_{\sigma_n(i)}. \quad (58)$$

Therefore, by the continuity of $x \mapsto \sqrt{x}$ it may be expected that

$$\sqrt{\sum_{k=1}^n \hat{N}_{i,k}} \approx \sqrt{\ell \pi(\sigma_n(i))\mu_{\sigma_n(i)}(i)} \quad \text{and} \quad \sqrt{\sum_{k=1}^n \hat{N}_{k,j}} \approx \sqrt{\ell \pi(\sigma_n(j))\mu_{\sigma_n(j)}(j)}. \quad (59)$$

The variance of a sum of independent random variables is equal to the sum of the variances. If we write $\hat{N}_{i,j} = \sum_{t=1}^{\ell-1} \mathbb{1}[X_t = i, X_{t+1} = j]$ then these summands are not independent but nonetheless we do expect the variance to approximately distribute over the sum. Therefore, it is expected that

$$\text{Var}[\hat{N}_{i,j}] \approx (\ell - 1) \text{Var}[\mathbb{1}[X_t = i, X_{t+1} = j]] = (\ell - 1) \pi(\sigma_n(i))\mu_{\sigma_n(i)}(i) p_{\sigma_n(i)\sigma_n(j)} \mu_{\sigma_n(j)}(j). \quad (60)$$

By combining (59) and (60) it follows that

$$\text{Var}[\hat{L}_{ij}] \approx \text{Var} \left[\frac{\hat{N}_{ij}}{\sqrt{\ell \pi(\sigma_n(i))\mu_{\sigma_n(i)}(i)} \sqrt{\ell \pi(\sigma_n(j))\mu_{\sigma_n(j)}(j)}} \right] \quad (61)$$

$$\approx \frac{\ell \pi(\sigma_n(i)) p_{\sigma_n(i)\sigma_n(j)} \mu_{\sigma_n(i)}(i) \mu_{\sigma_n(j)}(j)}{(\ell \pi(\sigma_n(i))\mu_{\sigma_n(i)}(i)) (\ell \pi(\sigma_n(j))\mu_{\sigma_n(j)}(j))} \quad (62)$$

$$= \ell^{-1} \pi(\sigma_n(j))^{-1} p_{\sigma_n(i)\sigma_n(j)} \quad (63)$$

$$\approx (\lambda n^2)^{-1} \pi(\sigma_n(j))^{-1} p_{\sigma_n(i)\sigma_n(j)} \quad (64)$$

Observe that this agrees with the variance profile which was used in Lemma 2.

14.4 Simulation experiment

We here measure the sensitivity of the spectral noise in \hat{L} and \hat{N} to violations of the model assumptions in the presence of an inhomogeneous equilibrium distribution by means of a perturbation to a DC-BMC model, defined in Supplement 14.3. The experiment is done by means of a simulation.

For the DC-BMC model we take $K = 2$ and we consider clusters of size $\#\mathcal{V}_1 = \#\mathcal{V}_2 = 1000$. The cluster transition matrix p is defined by $p_{11} = p_{22} = 0.8$ and $p_{12} = p_{21} = 0.2$. The probability measures μ_i are found for $i = 1, 2$ by sampling a vector of i.i.d. exponentially distributed random variables of rate 1 and normalizing this vector to have L^1 -norm equal to 1.

We may further consider a perturbation of this DC-BMC. Let Δ be a heavy-tailed transition matrix as defined in Section 3.2 and denote $P_{\text{perturbed}} := 0.95 P_{\text{DC-BMC}} + 0.05 \Delta$. Recall that the DC-BMC component $P_{\text{DC-BMC}}$ can be approximated with a BMC with more groups but note that such an approximation is not possible for Δ . Consequently, we may think of the decomposition for $P_{\text{perturbed}}$ as splitting the ground truth model into a main part which can be approximated with a BMC and a second part which requires a different explanation.

In the subsequent experiment we consider observation sequences $\{X_t\}_{t=1,\dots,\ell}$ and $\{Y_t\}_{t=0,\dots,\ell}$ with length $\ell = 2000^2$ from the DC-BMC-model and the perturbed model respectively. The singular value densities of the \hat{N} -matrix constructed from X and Y are displayed in Figure 11 (a). Also displayed in Figure 11 is the theoretical prediction corresponding to a BMC found by executing the clustering algorithm with $\tilde{K} = 4$ clusters. Recall that taking $\tilde{K} > K$ allows for the algorithm to split the groups to ensure that μ_i is roughly constant. We observe that the empirical densities associated to the DC-BMC-model and the perturbed model look quite similar apart from the fact that the perturbed model has a longer tail. The theoretical prediction associated to the BMC further provides an acceptable match for the DC-BMC model but there is also some small part of the tail of the DC-BMC model which escapes the theoretical prediction. Here the issue regarding the sensitivity of \hat{N} becomes apparent: there are at least two plausible explanations why in empirical data some part of the tail may escape the support of the theoretical density. A first explanation is the presence of a perturbation Δ which we view as a violation of the model assumptions. A second explanation is that the ground truth is a DC-BMC and one should take \tilde{K} to be larger. These two explanations are difficult to distinguish from the spectral noise in \hat{N} . In the current example one may argue that the amount of the tail which escapes the

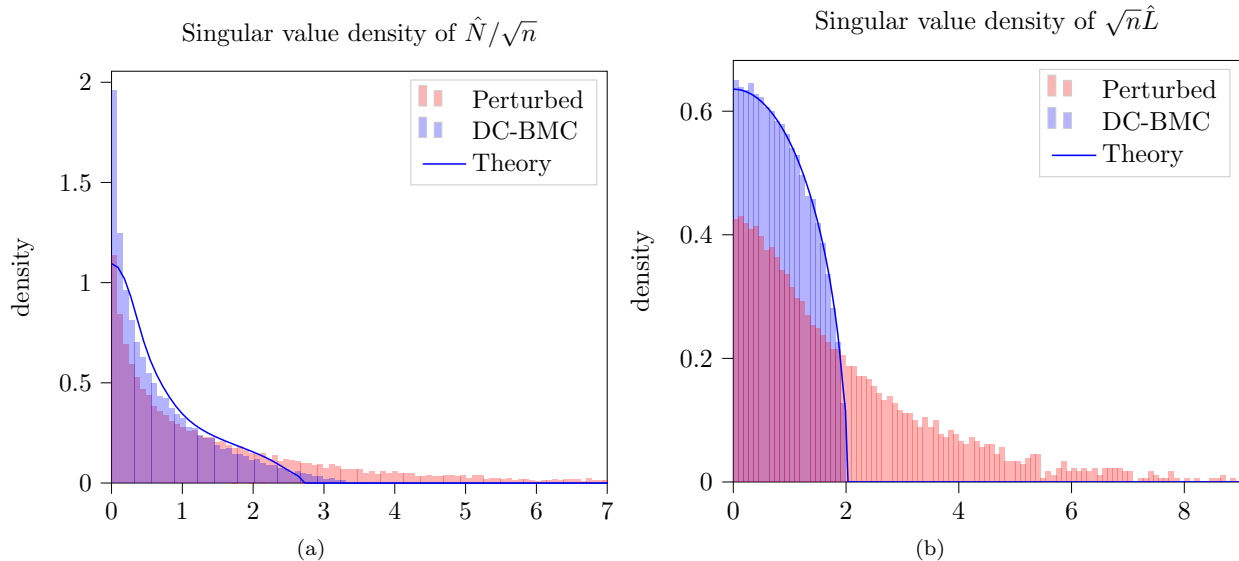


Fig. 11. (left) The singular value density of \hat{N} for a simulated DC-BMC (blue bars) as compared to the theory (blue line) and a perturbed model (red bars). (right) The singular value density of \hat{L} .

theoretical density is larger in the perturbed model. Such a judgement regarding the size of the tail is however undesirable since it is vague and subjective.

The singular value density of \hat{L} for the two sample paths $X_{1:\ell}$ and $Y_{1:\ell}$ is displayed in Figure 11 (b). Here we observe that the empirical densities of the DC-BMC model and the perturbed model are severely different. The theoretical prediction associated to the BMC moreover provides a good match to the DC-BMC model as was expected by the conjecture of Supplement 14.3. We conclude that the spectral noise in the Laplacian \hat{L} is more sensitive to violations of the model assumptions than the spectral noise in \hat{N} , particularly in the presence of an inhomogeneous equilibrium distribution.

15 Extra tools for some of the different data sets

15.1 The cf-idf vectorization method

Let \mathcal{V} denote the vocabulary, which is a set of words, and fix a clustering $\sigma_n : \mathcal{V} \rightarrow [K]$. In order to turn documents into vectors we make use of a straightforward modification of the common *term frequency-inverse document frequency* document vectorization method, we refer to the modification as *cluster frequency-inverse document frequency* (Cluster Frequency–Inverse Document Frequency). Let \mathcal{D} denote a collection of documents. Every document $d \in \mathcal{D}$ is here viewed as a sequence of words meaning that $d \in \prod_{t=1}^{\ell_d} \mathcal{V}$ for some $\ell_d > 0$. For every cluster $k \in [K]$ and document $d \in \mathcal{D}$ we define

$$\begin{aligned} \text{cf}(k, d) &:= \ln \left(1 + \#\{t = 1, \dots, \ell_d : \sigma_n(d_t) = k\} \right), \\ \text{idf}(k, \mathcal{D}) &:= \ln \left(\frac{\sum_{k=1}^K (1 + \sum_{d \in \mathcal{D}} \#\{t = 1, \dots, \ell_d : \sigma_n(d_t) = k\})}{1 + \sum_{d \in \mathcal{D}} \#\{t = 1, \dots, \ell_d : \sigma_n(d_t) = k\}} \right), \\ \text{cf-idf}(k, d) &:= \text{cf}(k, d) \cdot \text{idf}(k, \mathcal{D}). \end{aligned}$$

Observe that $\text{cf-idf}(\cdot, d)$ assigns a K -dimensional vector to any document $d \in \mathcal{D}$. A word which contributes multiple times in a document also yields a higher contribution of the corresponding cluster to $\text{cf}(k, d)$. Finally, words which are not in the vocabulary of the clustering are not counted at all in our processing.

15.2 Algorithm for creating a grid for animal movement data

Given a desired grid side length x (in kilometers), we can calculate the (regional) latitudinal and longitudinal degree corresponding to that distance x (assuming the earth to be a near perfect sphere). Latitudinal differences amount to the same distance in kilometers. One degree of latitude is 1/360th of the earth's circumference (40 075 km) so one degree of latitude is equivalent to 110.574 km. Accordingly, x km are represented by $x/110.574$ degrees of latitude. One degree of longitude however represents a different amount of kilometers, depending on the latitude: one degree of longitude is $|111.320 \cdot \cos_{\text{dd}}(\text{latitude})|$ km and x km are represented by $|x/111.320 \cdot \cos_{\text{dd}}(\text{latitude})|$ degrees of longitude, at a specific latitude. Here \cos_{dd} is the cosine acting on decimal degrees. We are making use of a small angle approximation, which breaks down near the poles. The process of creating squares and assigning the units y_i to them is done in the following Algorithm 3.

The algorithm assigns all the GPS points to squares. This procedure may not work well if the animal is moving close to the poles, because the small angle approximation is not justified anymore. This procedure is also not particularly well suited for regions where the earth is not behaving like a sphere, for example if the animal is moving on mountains.

Algorithm 3: GPS data to transitions between squares of side length x km

Input: Grid size x , GPS data $(y_{i1}, y_{i2}, y_{i3})_{i=1, \dots, n}$.
Output: Sequence of transitions between states $s = (s_1, \dots, s_n)$

```

1  $j_{\text{lat}} = \lfloor y_{11} \cdot 110.574/x \rfloor$ 
2  $j_{\text{long}} = \lfloor y_{12} \cdot 111.320 \cdot |\cos_{\text{dd}}(j_{\text{lat}} \cdot 110.574/x)|/x \rfloor$ 
3  $S_1 := \left[ j_{\text{lat}} \cdot \frac{x}{110.574}, (j_{\text{lat}} + 1) \cdot \frac{x}{110.574} \right) \times \left[ j_{\text{long}} \cdot \left| \frac{x}{111.320 \cdot \cos_{\text{dd}}(j_{\text{lat}} \cdot 110.574/x)} \right|, (j_{\text{long}} + 1) \cdot \left| \frac{x}{111.320 \cdot \cos_{\text{dd}}(j_{\text{lat}} \cdot 110.574/x)} \right| \right)$ 
4  $\mathcal{S} \leftarrow \{S_1\}$ 
5  $s \leftarrow (1)$ 
6 for  $\text{index}_{\text{coord}} \leftarrow 1$  to  $n$  do
7   for  $\text{index}_{\text{square}} \in \{1, 2, \dots, \#\mathcal{S}\}$  do
8      $\text{added} \leftarrow \text{False}$ 
9     if  $(y_{\text{index}_{\text{coord}}1}, y_{\text{index}_{\text{coord}}2}) \in S_{\text{index}_{\text{square}}}$  then
10        $s \leftarrow (s_1, \dots, s_{\text{index}_{\text{coord}}-1}, \text{index}_{\text{square}})$ 
11        $\text{added} \leftarrow \text{True}$ 
12     end
13     if  $\text{added} = \text{False}$  then
14        $j_{\text{lat}} = \lfloor y_{\text{index}_{\text{coord}}1} \cdot 110.574/x \rfloor$ 
15        $j_{\text{long}} = \lfloor y_{\text{index}_{\text{coord}}2} \cdot 111.320 \cdot |\cos_{\text{dd}}(j_{\text{lat}} \cdot 110.574/x)|/x \rfloor$ 
16        $S_{\#\mathcal{S}} := \left[ j_{\text{lat}} \cdot \frac{x}{110.574}, (j_{\text{lat}} + 1) \cdot \frac{x}{110.574} \right) \times \left[ j_{\text{long}} \cdot \left| \frac{x}{111.320 \cdot \cos_{\text{dd}}(j_{\text{lat}} \cdot 110.574/x)} \right|, (j_{\text{long}} + 1) \cdot \left| \frac{x}{111.320 \cdot \cos_{\text{dd}}(j_{\text{lat}} \cdot 110.574/x)} \right| \right)$ 
17        $\mathcal{S} \leftarrow \{S_1, \dots, S_{\#\mathcal{S}}\}$ 
18        $s \leftarrow (s_1, \dots, s_{\text{index}_{\text{coord}}-1}, \#\mathcal{S})$ 
19     end
20   end
21 end

```

16 Raw data of, and extra material on, some of the datasets

16.1 Transition matrix for bison clusters

Below is the cluster transition matrix for the improvement clustering depicted in Figure 6, the numbers are rounded to the second decimal place.

$$\begin{pmatrix} 0.82 & 0.05 & 0 & 0.01 & 0.02 & 0.01 & 0.01 & 0.01 & 0.02 & 0.02 & 0 & 0.01 & 0.01 & 0 & 0 \\ 0.07 & 0.76 & 0.02 & 0.03 & 0.05 & 0 & 0.01 & 0 & 0.01 & 0 & 0 & 0.02 & 0.02 & 0 & 0.01 \\ 0.01 & 0.05 & 0.87 & 0.03 & 0 & 0 & 0 & 0 & 0 & 0 & 0.03 & 0 & 0 & 0 & 0 \\ 0.02 & 0.06 & 0.03 & 0.85 & 0.03 & 0 & 0 & 0 & 0 & 0 & 0 & 0 & 0 & 0 & 0.01 \\ 0.04 & 0.07 & 0 & 0.02 & 0.77 & 0 & 0 & 0 & 0 & 0 & 0 & 0 & 0 & 0 & 0.1 \\ 0.04 & 0 & 0 & 0 & 0 & 0.88 & 0.02 & 0 & 0 & 0 & 0 & 0 & 0.03 & 0.02 & 0 \\ 0.03 & 0.01 & 0 & 0 & 0 & 0.01 & 0.86 & 0 & 0.01 & 0 & 0 & 0 & 0.04 & 0.03 & 0 \\ 0.06 & 0 & 0 & 0 & 0 & 0 & 0 & 0.84 & 0.07 & 0 & 0 & 0.01 & 0 & 0 & 0 \\ 0.09 & 0.01 & 0 & 0 & 0 & 0 & 0.01 & 0.06 & 0.72 & 0.01 & 0 & 0.1 & 0 & 0 & 0 \\ 0.06 & 0 & 0 & 0 & 0 & 0 & 0 & 0 & 0.01 & 0.79 & 0.1 & 0.03 & 0 & 0 & 0 \\ 0.01 & 0 & 0.04 & 0 & 0 & 0 & 0 & 0 & 0 & 0.09 & 0.83 & 0.02 & 0 & 0 & 0 \\ 0.03 & 0.06 & 0 & 0 & 0 & 0 & 0 & 0.01 & 0.1 & 0.04 & 0.02 & 0.73 & 0 & 0 & 0 \\ 0.03 & 0.06 & 0 & 0 & 0 & 0.04 & 0.05 & 0 & 0 & 0 & 0 & 0 & 0.77 & 0.05 & 0 \\ 0 & 0 & 0 & 0 & 0 & 0.05 & 0.07 & 0 & 0 & 0 & 0 & 0 & 0.14 & 0.72 & 0 \\ 0.02 & 0.03 & 0 & 0.01 & 0.31 & 0 & 0 & 0 & 0 & 0 & 0 & 0 & 0 & 0 & 0.63 \end{pmatrix}$$

16.2 Groups of words for improvement with 200 groups

16.2.1 Document classification datasets

We here describe the datasets which are used to construct Table 1 and report on some other datasets where our findings are inconclusive in Table 4.

16.2.1.1 AG News.: This dataset provided by [71] consists of tuples (x, y, z) where x is the title of a news article, y is a description of the news article and z is an assigned class. There are here four possible classes which z can take as values namely *World*, *Sports*, *Business* and *Sci/Tech*. For each such class the dataset contains precisely 30 000 training samples and 1 900 testing samples. In our processing we concatenated x and y into a single string and the task is to predict the class label z based on this string.

16.2.1.2 Yahoo!.: This dataset provided by [71] contains questions and answers from *Yahoo! answers*. The dataset consists of tuples (x, y_1, y_2, z) where x is a question, y_1, y_2 are answers to this question and z is category to which the question belongs. It can here also occur that the question has fewer than two answers in which case y_1 or y_2 is the empty string. There are ten possible classes which z can take as values namely *Society & Culture*, *Science & Mathematics*, *Health*, *Education & Reference*, *Computers & Internet*, *Sports*, *Business & Finance*, *Entertainment & Music*, *Family & Relationships* and *Politics & Government*. For each such class the dataset contains precisely 140 000 training samples and 5 000 testing samples. In our processing we concatenated x, y_1 and y_2 into a single string and the task is to predict the class label z based on this string.

16.2.1.3 Wiki.: This dataset comes from the DBpedia ontology project [65] and the precise version used here is constructed by [71]. The dataset consists of tuples (x, y, z) where x is a title of a Wikipedia page, y is the abstract of the page and z is the category to which the page belongs. There are 14 possible classes which z can take as values. For each such class the dataset contains precisely 40 000 training samples and 5 000 testing samples. In our processing we did not use the title x so the task is to predict the class label z based on the abstract y .

16.2.1.4 Book.: This dataset is constructed based on books from Project Gutenberg and their genres are assigned on GoodReads, the dataset was obtained from [68]. The dataset contains tuples (x, y, z) where x is the title of a book, y is the full text of this book and z contains a set of genres. We only retained those data points for which z is a set with a single element from one of the following six categories: *cookbooks*, *fantasy*, *horror*, *politics*, *religion* or *science-fiction*. We further randomly selected 2 000 training samples which left 387 samples for testing. In our processing we did not use the title x so the task is to predict the genre z based on the text y .

16.2.1.5 CMU.: The CMU Book Summary Dataset contains plot summaries for books which are extracted from Wikipedia by [60]. The dataset contains tuples (x, z) with x a plot summary and z the category to which the book belongs. We retain all datapoints whose category z occurs at least 50 times which leaves us with two genres namely *Fantasy* and *Science-Fiction*. We randomly select 1 138 datapoints for training which leaves us with 380 testing samples. The task is to predict the genre z based on the summary x .

16.2.1.6 20news.: This dataset contains newsgroup postings for 20 different newsgroups which are collected by [64]. The dataset is accessed using the function `fetch_20news` from `sklearn.datasets`. The dataset contains tuples (x, z) where x is a message sent to the newsgroup and z is the label of the newsgroup. There are 20 possible classes which z can take as values. There are 11 314 training samples and 7 532 testing samples. The task is to predict the newsgroup z given the message x .

16.2.1.7 Spam.: This dataset contains text messages which are either legitimate or spam, collected by [63], [62], [61]. The dataset is accessed from [58] and contains tuples (x, z) where x is a text message and z is a label indicating if the message is spam. The possible values for z are spam or ham. The task is to predict z given the message x . Unfortunately, due to a mistake, the experiment is executed without splitting the dataset in training and testing samples. This means that the 4 179 available samples are used both during training and testing. Splitting in testing and training would however not change the inconclusive conclusion from Table 4 and another experiment with a test-train split is not executed.

16.2.1.8 Reuters.: The Reuters RCV1 corpus [66] consists of a collection of news stories and was accessed using `nltk.download('reuters')`. The dataset contains tuples (x, z) with x a news article and z the category to which it belongs. There are 58 possible values for z . There are 6 577 training samples and 2 570 testing samples. The task is to predict the category z based on the text in x .

Algorithm	20news	Spam	Reuters
Random $K = 50$	23.2%	86.4%	65.4%
Spectral $K = 50$	23.0%	86.1%	63.0%
Improved $K = 50$	25.2%	86.1%	63.3%
Random $K = 100$	31.0 %	86.7%	67.7%
Spectral $K = 100$	31.1%	86.9%	66.2%
Improved $K = 100$	33.6%	87.2%	68.9%
Random $K = 200$	38.0%	87.2%	68.4%
Spectral $K = 200$	36.2%	87.0%	69.0%
Improved $K = 200$	40.2%	87.2%	70.8%
Random $K = 400$	44.7%	87.6%	87.8%
Spectral $K = 400$	41.4%	87.7%	88.0%
Improved $K = 400$	43.9%	87.7%	89.0%

TABLE 4

Results for performance on document classification where neither method significantly outperformed a random clustering.

16.2.2 Detected groups

Here are the detected groups when using the cluster improvement algorithm:

- V₅₀ = founder, deputi, formerli, mayor, bishop, meanwhile, successor, chose, chairman, admir, lincoln, advis, secretari, fellow, hire, cabinet, crown, invit, inaugur, ceo, scout, editor, politician, resign, lawyer, colonel, journalist, assassin, mp, veteran, lieuten, architect, chair, rival, renam, presidenti, briefli, victoria, commission, attorney,
 V₅₁ = tonn, usd, capita, lb, ton, ago, liter, cubic, cent, trillion, exceed, metric, kilomet, €, pound, gram, annum, dollar, revol, yen, fifti, euro, kg, kilogram, crore, gallon, kilometr, se, gdp, weigh, acr, gross, hectar, rs,
 V₅₂ = cavalli, jet, helicopt, rifl, warfar, battalion, raid, assault, naval, airborne, artilleri, fleet, bomber, missil, guard, strateg, squadron, submarin, regiment, patrol, expedit, fighter, corp, deploy, infantri, brigad, armour, carrier, combat, tactic, aviat, personnel, armor,
 V₅₃ = egyptian, portugues, polish, welsh, palestinian, vice, austrian, commonwealth, oversea, nazi, puerto, dutch, czech, scottish, confeder, swiss, hungarian, tamil, continent, merchant, sri, turkish, mexican, irish, iranian, danish, isra, belgian, imperi, swedish, norwegian, provinci, brazilian,
 V₅₄ = behavior, mental, cancer, brain, emot, neg, therapi, symptom, psycholog, compound, diseas, abus, clinic, seriou, ill, reaction, depress, gene, treatment, surgeri, biolog, pain, stress, treat, patient, sexual, infect, chemic, disord, failur, genet, risk,
 V₅₅ = via, variet, link, extens, construct, flight, ground, manufactur, store, transport, equip, ship, access, distribut, suppli, rang, facil, space, avail, format, free, commerci, car, weapon, fire, aircraft, food, comput, plant, vehicl, connect,
 V₅₆ = coverag, regularli, hollywood, comedi, disney, logo, weekli, anchor, amateur, serial, daili, theater, fox, fm, poll, documentari, realiti, bbc, cancel, holiday, venu, affili, franchis, drama, nbc, mail, syndic, sky, cb, abc, cartoon,
 V₅₇ = brief, genr, adventur, tape, disc, photo, compil, biggest, cd, soundtrack, mainstream, dvd, hero, entitl, highlight, signatur, lyric, favorit, ep, christma, audio, certifi, lineup, fantasi, tune, greatest, session, sing, solo, string,
 V₅₈ = civilian, jew, citizen, occup, immigr, egypt, era, affair, regim, pakistan, occupi, tribe, settl, settlement, soldier, republ, coloni, israel, airlin, allianc, invas, slave, flag, revolt, alli, troop, camp, philippin, rome, navi,
 V₅₉ = previous, soon, simpli, refus, heart, frequent, better, yet, longer, might, hope, agre, actual, intend, commonli, —, here, hard, immedi, unabl, expect, ultim, quickli, alway, already, fail, ever, probabl,
 V₆₀ = miss, crew, schedul, youth, challeng, elimin, prior, entri, incid, beat, lose, struggl, driver, strike, compet, owner, crime, offens, enemi, shoot, partner, defend, draw, contest, tie, latter,
 V₆₁ = abl, claim, doe, must, hand, upon, attempt, still, need, action, order, initi, without, onc, instead, find, should, decid, help, never, right, plan, event, tri,
 V₆₂ = softwar, advertis, joint, licens, rail, microsoft, transit, onlin, web, instal, digit, mobil, camera, bu, traffic, satellit, platform, window, cabl, phone, passeng, termin, internet,
 V₆₃ = appar, desir, fulli, lot, increasingli, highli, beyond, quit, understand, difficult, prove, perhap, easili, clear, rare, danger, sex, awar, necessari, extrem, tend,
 V₆₄ = stop, stand, keep, behind, taken, brought, escap, travel, drop, destroy, fall, rest, discov, captur, sent, save, arriv, bring, visit, drive, stay, put,
 V₆₅ = orchestra, hop, acoust, symphoni, hip, guitarist, vocalist, bass, folk, drum, guitar, vocal, keyboard, warner, rb, punk, jazz, pop, rhythm, piano, songwrit,
 V₆₆ = japan, canada, territori, zealant, germani, europ, spain, mexico, england, ireland, kingdom, franc, australia, border, china, capit, russia, provinc, itali, scotland, pari,
 V₆₇ = dont, think, seem, ask, want, told, feel, felt, happen, realli, done, someth, thought, am, let, know, talk, explain, tell, got,
 V₆₈ = concentr, profil, elev, capac, extent, ratio, yield, significantli, domain, incom, output, quantiti, densiti, sum, percentag, slightli, frequenc, effici, volt, proport,
 V₆₉ = bridg, villag, road, front, hill, site, templ, section, street, middl, outsid, rout, valley, mountain, centr, cross, resid, port, nativ,
 V₇₀ = again, led, return, die, sign, join, leav, replac, meet, attack, togeth, begin, enter, left, lost, reach, kill, held, mark,
 V₇₁ = younger, husband, historian, succeed, alongsid, saint, reign, ladi, lord, queen, emperor, pope, portray, sir, mr, dr, le, captain, princ,
 V₇₂ = boy, king, wife, parent, friend, son, murder, marri, father, met, brother, woman, girl, mother, daughter, marriag, sister, whom, child,
 V₇₃ = soap, bueno, thth, fifteenth, buckingham, sixteenth, tampa, nineteenth, fourteenth, thirteenth, eleventh, midth, twentieth, twentyfirst, twilight, eighteenth, twelfth, pga, seventeenth,
 V₇₄ = sinc, origin, member, success, appear, live, life, them, group, against, histori, peopl, home, famili, seri, show, countri, perform,
 V₇₅ = park, side, along, region, across, river, western, central, london, built, northern, town, eastern, island, near, locat, throughout, southern,
 V₇₆ = undergradu, cambridg, oldest, oxford, lectur, bachelor, faculti, enrol, graduat, phd, professor, lectur, scholarshp, nurs, campu, harvard, galleri,
 V₇₇ = legisl, administr, seat, committe, congress, vote, parliament, campaign, opposit, commiss, council, leader, governor, senat, bill, candid, assembl,
 V₇₈ = june, born, february, novemb, august, januari, career, juli, septemb, forc, york, decemb, march, april, octob, announc, began,
 V₇₉ = given, person, allow, result, becaus, consid, veri, even, refer, among, describ, mean, give, see, make, caus, due,
 V₈₀ = oil, spread, upper, urban, climat, lie, portion, agricultur, ga, zone, farm, forest, surround, bay, wind, flow, mine,
 V₈₁ = sunday, monday, saturday, pm, walt, tuesday, afterward, wednesday, weekend, shortli, friday, thereaft, weekday, morn, thursday, afternoon, newscast,
 V₈₂ = medici, bayern, aston, jure, plata, liga, facto, sall, moin, atlético, rothschild, havilland, janeiro, palma, vega, versail, gaul,
 V₈₃ = b, c, x, v, iii, g, e, r, f, j, d, k, p, l, w, h,
 V₈₄ = next, summer, previou, ten, hour, five, everi, nine, seven, six, eight, big, hall, night, entir, few,
 V₈₅ = research, commun, servic, inform, studi, scienc, educ, organ, econom, center, institut, polit, busi, program, train, social,
 V₈₆ = elizabeth, loui, arthur, alexand, stephen, patrick, martin, mari, philip, joseph, lawrenc, andrew, franci, edward, ann, duke,
 V₈₇ = blood, gun, light, tree, wing, room, eye, sea, machin, surfac, heavi, color, earth, metal, wall, fish,
 V₈₈ = draft, nba, pick, rugbi, nfl, squad, junior, winner, tournament, playoff, qualifi, confer, ncaa, retir, senior,
 V₈₉ = christian, greek, thousand, latin, arab, protest, islam, muslim, hundr, speak, minor, translat, ancient, religion, jewish,
 V₉₀ = exchang, sold, acquir, invest, sale, brand, purchas, sell, transfer, corpor, global, fund, pay, stock, privat,
 V₉₁ = true, thing, littl, idea, your, question, my, whether, how, our, look, fact, god, too, me,
 V₉₂ = famou, note, write, list, short, wrote, danc, classic, compos, collect, notabl, read, written, cover,
 V₉₃ = justic, investig, appeal, judg, crimin, approv, declar, constitut, peac, decis, arrest, prison, trial, grant,
 V₉₄ = avoid, damag, prevent, suffer, affect, grow, potenti, poor, resist, loss, drug, injuri, strong, lack,
 V₉₅ = languag, cultur, practic, word, relat, view, interest, histor, movement, influenc, associ, modern, tradit, societi,
 V₉₆ = russian, indian, french, canadian, german, australian, spanish, royal, english, foreign, italian, japanes, chines,
 V₉₇ = differ, small, larg, main, ani, close, similar, import, popular, common, good, variou, increas,
 V₉₈ = charl, john, georg, robert, michael, jame, paul, david, william, henri, thoma, peter, richard,
 V₉₉ = twoyear, lockhe, rhode, oneyear, rio, virgin, zeppelin, fouryear, threeyear, amus, sponsorship, fiveyear,
 V₁₀₀ = athlet, pro, cricket, basebal, profession, wrestl, soccer, bowl, basketbal, hockey, super, stadium,
 V₁₀₁ = final, start, late, second, end, four, earli, until, last, befor, three,
 V₁₀₂ = price, speed, level, energi, pressur, temperatur, degre, rate, water, cell, cost,
 V₁₀₃ = stage, fight, defeat, race, club, battl, victori, player, competit, match, win,
 V₁₀₄ = pass, come, turn, go, came, get, run, date, just, move, went,
 V₁₀₅ = fa, afc, stanley, middleweight, fifa, intercontinent, sprint, nfc, uefa, heavyweight, costa,
 V₁₀₆ = charact, book, music, role, featur, stori, star, titl, direct, version,
 V₁₀₇ = larger, less, below, greater, higher, smaller, abov, reduc, lower, low,
 V₁₀₈ = so, i, we, could, what, do, did, you, if, like,
 V₁₀₉ = negoti, firm, provis, proceed, jurisdict, impos, amend, violat, prohibit, enforc,
 V₁₁₀ = prize, outstand, honor, silver, honour, bronz, ceremoni, medal, golden,
 V₁₁₁ = channel, movi, launch, host, entertain, news, media, broadcast, sport,
 V₁₁₂ = consecut, eighth, tenth, ninth, seventh, rd, sixth, fifth, nd,
 V₁₁₃ = children, himself, young, man, women, age, men, death, old,
 V₁₁₄ = annual, total, tax, percent, highest, rise, estim, averag, growth,
 V₁₁₅ = socialist, reform, labour, communist, liber, democrat, republican, labor, conserv,
 V₁₁₆ = former, attend, chief, assist, elect, board, serv, head, appoint,
 V₁₁₇ = spent, roughli, almost, squar, spend, approxim, worth, nearli, £,
 V₁₁₈ = academ, environment, scientif, technic, medic, primari, financi, health, secondari,
 V₁₁₉ = outbreak, gulf, vietnam, cold, iraq, korean, tag, revolutionari,
 V₁₂₀ = establish, offic, church, rule, offic, author, independ, parti,
 V₁₂₁ = ball, roll, walk, cut, step, break, shot,
 V₁₂₂ = weight, size, length, distanc, enough, scale, amount,
 V₁₂₃ = indi, korea, asian, coast, wale, asia, carolina,
 V₁₂₄ = doubl, femal, male, promin, adult, guest, cast,
 V₁₂₅ = champion, cup, premier, coach, footbal, championship,
 V₁₂₆ = song, top, singl, album, track, band,
 V₁₂₇ = command, polic, staff, execut, post, box,
 V₁₂₈ = green, white, red, blue, black, gold,
 V₁₂₉ = hit, uk, studio, concert, debut, tour,
 V₁₃₀ = versa, latterday, rico, nadu, rica, rican,

131	=	y, grand, et, del, el, al,
132	=	say, said, 'l, believ, love,
133	=	museum, contemporari, fine, master, martial,
134	=	american, west, east, south, north,
135	=	america, africa, india, african, bank,
136	=	singer, musician, actress, writer, actor,
137	=	secur, task, defens, reserv, defenc,
138	=	through, back, away, down, off,
139	=	third, regular, finish, rank, fourth,
140	=	half, largest, round, decad, quarter,
141	=	now, becom, best, becam, well,
142	=	artist, rock, style, director, video,
143	=	olymp, theatr, festiv, airport, trade,
144	=	yard, field, score, touchdown, goal,
145	=	prix, juri, slam, duchi, testament,
146	=	motor, magnet, real, nuclear, electr,
147	=	million, around, popul, us,
148	=	british, union, presid, govern,
149	=	earl, birthday, grade, anniversari,
150	=	univers, art, law, student,
151	=	billboard, hot, peak, chart,
152	=	usual, often, thu, sometim,
153	=	season, leagu, war, team,
154	=	fiction, technolog, polici, care,
155	=	recept, review, prais, acclaim,
156	=	francisco, angel, diego, kong,
157	=	divis, minut, overal,
158	=	militari, armi, depart,
159	=	opera, marin, palac,
160	=	nomin, academi, won,
161	=	n, m, t,
162	=	lake, britain, deal,
163	=	long, much, far,
164	=	determin, vari, depend,
165	=	known, took, take,
166	=	agreement, contract, treati,
167	=	copi, billion, per,
168	=	televis, episod, tv,
169	=	day, month, week,
170	=	washington, district, suprem,
171	=	soviet, feder, european,
172	=	religi, indigen, ethnic,
173	=	counti, colleg, california,
174	=	mid, bc,
175	=	critic, posit,
176	=	retain, assum,
177	=	ottoman, roman,
178	=	minist, prime,
179	=	ii, civil,
180	=	radio, railway,
181	=	de, la,
182	=	air, arm,
183	=	comic, publish,
184	=	columbia, dc,
185	=	station, network,
186	=	lanka, lankan,
187	=	cathol, empir,
188	=	court, school,
189	=	high, public,
190	=	lo, hong,
191	=	“, ”,
192	=	st,
193	=	san,
194	=	fame,
195	=	award,
196	=	place,
197	=	wide,
198	=	centuri,
199	=	th,
200	=	∅

16.3 Companies with the highest daily returns

16.3.1 Sector breakdown within the S&P500 and the dataset

Table 5 contains the sector breakdown within the dataset as well as the S&P500. These numbers are based on S&P500's factsheet from 2022.

16.3.2 Ticker symbols of the 300 constituents

Here are the ticker symbols of the 300 companies that we considered, in order:

∇ = IP, CB, ZBH, AAPL, GS, IBM, AMGN, MMM, CVX, FDX, COST, CMI, UNP, AVB, BLK, SPG, HD, LMT, JNJ, KMB, JPM, GD, MCK, ESS, CI, UNH, CSCO, PXD, MCD, NVDA, INTC, PSA, MTB, HON, BXP, GWW, NOC, TMO, BA, INTU, APD, TRV, RTX, PEP, CAT, AMAT, TXN, ORCL, WHR, BDX, PPG, QCOM, SHW, UPS, PH, LRCX, PFE, NSC, HUM, ECL, DE, ADF, GE, SRE, ROK, WMT, EOG, MLM, PG, RE, DIS, NEE, T, ITW, KLAG, XOM, PNC, RL, AON, EA, LOW, BAC, AXP, VZ, GMCSA, SYR, EBAY, STZ, WFC, HPG, ROP, AMT, ABT, CLX, BEN, C, LLY, SNA, SWK, MS, CTXS, KSU, MCO, MRK, EL, FRT, KO, HAL, APA, WM, SJM, ADI, DHR, FCX, JCI, VMC, MSI, IFF, SBUX, GILD, CTAS, CVS, ALL, UHS, COO, SLB, MMC, TT, MCHP, NLOK, MDT, HSY, TGT, BMY, TROW, NKE, USB, COP, EFX, XLNX, MO, DRI, ROST, DTE, JNPR, CCI, BBY, NTAP, DUK, OXY, TFX, VLO, LHX, FAYX, FITB, SBAC, ETR, GPS, COF, NEM, MRO, KR, YUM, CL, DD, DGX, WBA, SCHW, MAR, GLW, SO, BK, JBHT, NTRS, PGR, TJX, AIG, ADM, HWM, A, CAC, STT, SY, HES, ABC, DOV, CSX, EIX, GIS, IFC, WMB, NUE, VFC, ETN, BAX, EMI, EXC, JKH, CAH, AEP, AFL, XEL, TECH, ATVI, ARE, DVN, HIG, AVY, NWL, WY, OMC, PCAR, FE, D, MAS, POOL, LEN, BBWI, VNO, EQR, NI, TER, CPB, DHI, PEG, K, LUMN, PPL, HAS, MU, MKC, PLD, LNC, ZION, ED, APH, MGM, CNP, PVH, CMA, CTSH, EMN, FAST, TSN, IEX, RSG, AEE, EXPD, TSCO, TXT, ES, CINF, MOS, CHRW, CERN, PFGT, RGL, UDR, CTRA, PEAK, TAP, CCL, SEE, KIM, ALB, KEY, XRAY, RMD, STE, DRE, BWA, WEC, RHI, GPC, FMC, L, J, LEG, OKE, MAA, CMS, PHM, VTR, IRM, PRI, O, ODFL, SWKS, AES, HRL, BLL, AME, AJG, LVZ, RJF, PNR, GL, LUV, IPG, FNW.

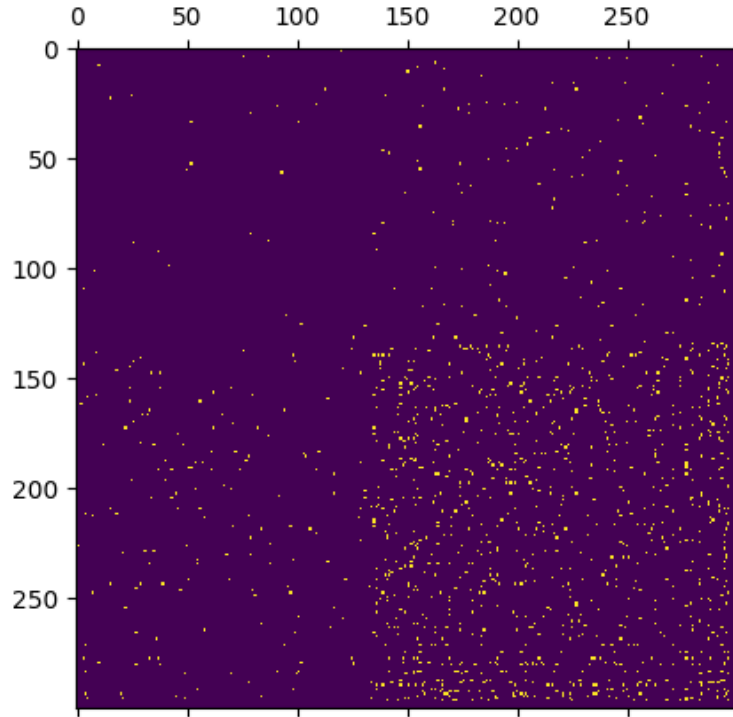


Fig. 12. A plot of the matrix $\{1[\hat{F}_{ij} > 0]\}_{i,j}$, where the rows and columns are sorted according to the improved clustering. We plotted the matrix like such because \hat{F} is quite sparse due to the trajectory's length $\ell = 2451$ being quite short: the minimum, median, mean, and maximum of the entries of the matrix $\{\hat{F}_{i,j}\}_{i,j}$ are 0, 0, $\ell/n^2 \approx 0.027$, and 14, respectively.

ESS (Real Estate), CSCO (Information Technology), INTC (Information Technology), PSA (Real Estate), MTB (Financials), HON (Industrials), BXP (Real Estate), GWW (Industrials), NOC (Industrials), BA (Industrials), APD (Materials), TRV (Financials), RTX (Industrials), PEP (Consumer Staples), CAT (Industrials), AMAT (Information Technology), BDX (Health Care), PPG (Materials), SHW (Materials), UPS (Industrials), PH (Industrials), PFE (Health Care), NSC (Industrials), ECL (Materials), DE (Industrials), ADP (Information Technology), GE (Industrials), SRE (Utilities), WMT (Consumer Staples), PG (Consumer Staples), DIS (Communication Services), NEE (Utilities), T (Communication Services), ITW (Industrials), XOM (Energy), PNC (Financials), BAC (Financials), AXP (Financials), VZ (Communication Services), SYK (Health Care), CLX (Consumer Staples), BEN (Financials), C (Financials), LLY (Health Care), SNA (Industrials), FRT (Real Estate), KO (Consumer Staples), AFA (Energy), WM (Industrials), DHR (Health Care), IFF (Materials), CVS (Health Care), ALL (Financials), TT (Industrials), MDT (Health Care), BMY (Health Care), NKE (Consumer Discretionary), COP (Energy), EFX (Industrials), DTE (Utilities), DUK (Utilities), OXY (Energy), ETR (Utilities), KR (Consumer Staples), YUM (Consumer Discretionary), CL (Consumer Staples), DD (Materials), DGX (Health Care), WBA (Consumer Staples), SO (Utilities), BK (Financials), NTRS (Financials), CAG (Consumer Staples), SYU (Consumer Staples), DOV (Industrials), EIX (Utilities), GIS (Consumer Staples), TFC (Financials), ETN (Industrials), BAX (Health Care), EMR (Industrials), EXC (Utilities), AEP (Utilities), AFL (Financials), ARE (Real Estate), AVY (Materials), OMC (Communication Services), FE (Utilities), D (Utilities), VNO (Real Estate), EQR (Real Estate), NI (Utilities), CPB (Consumer Staples), PEG (Utilities), K (Consumer Staples), LUMN (Communication Services), PPL (Utilities), HAS (Consumer Discretionary), MKC (Consumer Staples), ED (Utilities), EMN (Materials), RSG (Industrials), AEE (Utilities), ES (Utilities), CINF (Financials), UDR (Real Estate), CCL (Consumer Discretionary), XRAY (Health Care), WEC (Utilities), GPC (Consumer Discretionary), L (Financials), OKE (Energy), MAA (Real Estate), O (Real Estate), BLL (Materials), AJG (Financials), PNR (Industrials), GL (Financials), PNW (Utilities)

$\mathcal{V}_2 =$ IP (Materials), ZBH (Health Care), CMI (Industrials), BLK (Financials), LMT (Industrials), MCK (Health Care), CI (Health Care), UNH (Health Care), PXD (Energy), MCD (Consumer Discretionary), TMO (Health Care), INTU (Information Technology), TXN (Information Technology), ORCL (Information Technology), WHR (Consumer Discretionary), QCOM (Information Technology), ROK (Industrials), EOG (Energy), MLM (Materials), RE (Financials), KLAC (Information Technology), RL (Consumer Discretionary), AON (Financials), EA (Communication Services), LOW (Consumer Discretionary), CMCSA (Communication Services), EBAY (Consumer Discretionary), STZ (Consumer Staples), WFC (Financials), HPQ (Information Technology), ROP (Industrials), ABT (Health Care), SWK (Industrials), MS (Financials), CTXS (Information Technology), KSU (Industrials), MCO (Financials), MRK (Health Care), EL (Consumer Staples), SJM (Consumer Staples), ADI (Information Technology), JCI (Industrials), VMC (Materials), MSI (Information Technology), SBUX (Consumer Discretionary), GILD (Health Care), CTAS (Industrials), UHS (Health Care), SLB (Energy), MMC (Financials), MCHP (Information Technology), NLOK (Information Technology), HSY (Consumer Staples), TGT (Consumer Discretionary), TROW (Financials), USB (Financials), XLNX (Information Technology), MO (Consumer Staples), DRI (Consumer Discretionary), ROST (Consumer Discretionary), BBY (Consumer Discretionary), TFX (Health Care), LHX (Industrials), PAXX (Information Technology), GPS (Consumer Discretionary), COF (Financials), MRO (Energy), SCHW (Financials), MAR (Consumer Discretionary), JBHT (Industrials), PGR (Financials), TJX (Consumer Staples), ADM (Consumer Staples), HWM (Industrials), A (Health Care), STT (Financials), HES (Energy), ABC (Health Care), CSX (Industrials), NUE (Materials), VFC (Consumer Discretionary), JKHY (Information Technology), CAH (Health Care), XEL (Utilities), TECH (Health Care), DVN (Energy), HIG (Financials), NWL (Consumer Discretionary), WY (Real Estate), PCAR (Industrials), MAS (Industrials), POOL (Consumer Discretionary), BBWI (Consumer Discretionary), DHI (Consumer Discretionary), PLD (Real Estate), LNC (Financials), ZION (Financials), APH (Information Technology), CNP (Utilities), CMA (Financials), CTSH (Information Technology), FAST (Industrials), IEX (Industrials), EXPD (Industrials), TSCO (Consumer Discretionary), TXT (Industrials), CHRW (Industrials), CERN (Health Care), PBCT (Financials), RCL (Consumer Discretionary), CTRA (Energy), PEAK (Real Estate), TAP (Consumer Staples), SEE (Materials), KIM (Real Estate), ALB (Materials), KEY (Financials), RMD (Health Care), STE (Health Care), DRE (Real Estate), BWA (Consumer Discretionary), RHI (Industrials), FMC (Materials), J (Industrials), LEG (Consumer Discretionary), CMS (Utilities), VTR (Real Estate), IRM (Real Estate), PKI (Health Care), HRL (Consumer Staples), AME (Industrials), IVZ (Financials), RJF (Financials), LUV (Industrials)

$\mathcal{V}_3 =$ AAPL (Information Technology), NVDA (Information Technology), LRCX (Information Technology), HUM (Health Care), AMT (Real Estate), HAL (Energy), FCX (Materials), COO (Health Care), JNPR (Information Technology), CCI (Real Estate), NTAP (Information Technology), VLO (Energy), FTB (Financials), SBAC (Real Estate), NEM (Materials), GLW (Information Technology), AIG (Financials), WMB (Energy), ATVI (Communication Services), LEN (Consumer Discretionary), TER (Information Technology), MU (Information Technology), MGM (Consumer Discretionary), PVH (Consumer Discretionary), TSN (Consumer Staples), MOS (Materials), PHM (Consumer Discretionary), ODFL (Industrials), SWKS (Information Technology), AES (Utilities), IPG (Communication Services)

Supplementary Material Literature

- [58] Tiago A. Almeida and Jose Maria Gomez Hidalgo. SMS Spam Collection Data Set. <https://www.kaggle.com/datasets/uciml/sms-spam-collection-dataset>.
- [59] Zhidong Bai and Jack W Silverstein. *Spectral Analysis of Large Dimensional Random Matrices*. 2010.
- [60] David Bamman and Noah A Smith. New Alignment Methods for Discriminative Book Summarization. *arXiv preprint arXiv:1305.1319*, 2013. Accessed at <https://www.kaggle.com/datasets/yamaricar/cmu-book-summary-dataset>.
- [61] Gordon V. Cormack, José María Gómez Hidalgo, and Enrique Puertas Sáenz. Spam Filtering for Short Messages. In *Proceedings of the sixteenth ACM conference on Conference on information and knowledge management*, 2007.
- [62] Gordon V. Cormack, José María Gómez Hidalgo, and Enrique Puertas Sáenz. Feature Engineering for Mobile (SMS) Spam Filtering. In *Proceedings of the 30th annual international ACM SIGIR conference on Research and development in information retrieval*, 2007.

- [63] José María Gómez Hidalgo, Guillermo Cajigas Bringas, Enrique Puertas Sáenz, and Francisco Carrero García. Content based SMS spam filtering. In *Proceedings of the 2006 ACM symposium on Document engineering*, 2006.
- [64] Ken Lang. NewsWeeder: Learning to Filter Netnews. In *Proceedings of the Twelfth International Conference on Machine Learning*, 1995.
- [65] Jens Lehmann, Robert Isele, Max Jakob, Anja Jentzsch, Dimitris Kontokostas, Pablo N Mendes, Sebastian Hellmann, Mohamed Morsey, Patrick Van Kleef, Sören Auer, and Christian Bizer. DBpedia – A Large-scale, Multilingual Knowledge Base Extracted from Wikipedia. *Semantic web*, 2015.
- [66] David D. Lewis, Yiming Yang, Tony Russell-Rose, and Fan Li. RCV1: A New Benchmark Collection for Text Categorization Research. *Journal of machine learning research*, 2004.
- [67] Daniel Paulin. Concentration inequalities for Markov chains by Marton couplings and spectral methods. *Electronic Journal of Probability*, 2015.
- [68] Mike Russel. 10.000 Books and Their Genres standardized. Accessed at <https://www.kaggle.com/code/michaelrussell4/gutenberg-book-genre-feature-engineering/data>, 2021.
- [69] Jaron Sanders, Alexandre Proutière, and Se-Young Yun. Clustering in Block Markov Chains. *The Annals of Statistics*, 2020.
- [70] Jaron Sanders and Alexander Van Werde. Singular value distribution of dense random matrices with block Markovian dependence. *arXiv preprint arXiv:2204.13534*, 2022.
- [71] Xiang Zhang, Junbo Zhao, and Yann LeCun. Character-level Convolutional Networks for Text Classification. *Advances in Neural Information Processing Systems*, 2015.